

Propellant Throughput Capability of the Dawn Ion Thrusters

IEPC-2007-279

Presented at the 30th International Electric Propulsion Conference, Florence, Italy
September 17-20, 2007

John R. Brophy*

Jet Propulsion Laboratory,
California Institute of Technology, Pasadena, CA 91101, USA

Dawn, a mission to rendezvous with the main-belt asteroids Vesta and Ceres, is the first NASA science mission to use ion propulsion. The Dawn ion propulsion system is used to provide all post-launch ΔV . The ion propulsion system, which includes three 30-cm ion thrusters operated one at a time, is required to be single fault tolerant. The loss of a single thruster at the beginning of the mission requires that the mission be successfully completed with the remaining two thrusters. This paper assesses the mission risk due to wear-out failures of these remaining two thrusters. Extensive long-duration testing suggests that all of the important wear-out failure modes are known for the Dawn ion thrusters. The life-limiting failure mode is known to be electron-backstreaming due to erosion by charge-exchange ions. Since this failure mode that cannot be easily mitigated for Dawn, understanding its behavior is essential for assessing its impact on mission risk. Detailed analyses, both deterministic and probabilistic, are presented which show that this wear-out failure mode should not pose a significant risk to the success of the mission. The probability of a wear-out failure due to accelerator grid erosion is less than 1% for the worst-case mission use of the ion thrusters.

Nomenclature

| | | |
|--------------|---|--------------------------------|
| d_a | = | accelerator grid hole diameter |
| d_b | = | beamlet diameter |
| d_s | = | screen grid hole diameter |
| e | = | electron charge |
| J_b | = | beamlet current |
| J_e | = | backstreaming electron current |
| l_e | = | effective acceleration length |
| l_g | = | grid separation length |
| m_e | = | electron mass |
| m_i | = | ion mass |
| t_a | = | accelerator grid thickness |
| t_s | = | screen grid thickness |
| T_e | = | electron temperature |
| V_a | = | accelerator grid voltage |
| V_{bp} | = | beam plasma potential |
| V_{sp} | = | saddle-point voltage |
| ϵ_0 | = | permittivity of free space |

* Project Element Manager, Propulsion and Materials Engineering Section, John.R.Brophy@jpl.nasa.gov.

I. Introduction

Dawn is the ninth project in NASA's Discovery Program. The Dawn spacecraft is being developed to enable the scientific investigation of the two heaviest main-belt asteroids, (4) Vesta and (1) Ceres [1]. To accomplish this investigation the spacecraft will rendezvous with and go into orbit about each of these asteroids. Dawn will be the first mission to orbit two different extraterrestrial (and nonsolar) bodies, and the first to orbit a main-belt asteroid. The mission is enabled by Dawn's ion propulsion system which provides all of the post-launch ΔV including the heliocentric transfer to Vesta, orbit capture at Vesta, transfer between Vesta science orbits, departure and escape from Vesta, heliocentric transfer to Ceres, orbit capture at Ceres, and transfer between Ceres science orbits. The ion propulsion system provides a total ΔV of over 11 km/s to the Dawn spacecraft which has an initial wet mass of 1219 kg including 425 kg of xenon.

The Dawn ion propulsion system includes three 30-cm diameter xenon ion thrusters and two Power Processor Units (PPUs) of the type developed by the NSTAR Project [2] and flight-tested on NASA's Deep Space 1 (DS1) mission [3-5]. The IPS also includes two Digital Control & Interface Units (DCIUs), a xenon feed system (XFS), and three 2-axis thruster-gimbal assemblies (TGAs) – one for each ion thruster. A new light-weight xenon tank design developed specifically for Dawn is used to store 425 kg of xenon. In addition to the xenon tank, the xenon feed system includes two plenum tanks identical to those flown on DS1, a xenon control assembly (XCA) that uses the same propellant flow rate control technology demonstrated on DS1, a high-pressure subassembly that isolates the xenon tank from the rest of the feed system, nine service valves, all the interconnecting tubing, and nine flexible propellant lines (three for each thruster to go across the gimbal interface). The two PPU's are cross strapped to the three ion thrusters in such a way that PPU-A can operate either Flight Thruster-1 (FT1) or Flight Thruster-3 (FT3), and PPU-B can operate either Flight Thruster-2 (FT2) or Flight Thruster-3 (FT3) as indicated in Fig. 1. The high-voltage harnesses are indicated by the red lines in this figure. Since FT3 can be operated by either PPU it is referred to as the "shared" thruster. Each PPU includes a bank of high-voltage relays that switch the power supply outputs between the two thrusters. Each PPU is controlled by a dedicated DCIU, i.e., DCIU-A controls PPU-A only, and DCIU-B controls PPU-B only. Each DCIU, however, can control all the valves in the xenon feed system and all of the actuators in the three TGAs. The Dawn IPS operates only one ion thruster at a time.

The IPS for Dawn is required to be single-fault-tolerant. To meet this requirement the IPS must be capable of performing the entire mission even if one thruster is inoperable for any reason right from the start of the mission. This situation represents the worst-case mission use for the thrusters in which the entire mission is performed with just the two remaining thrusters. This paper addresses the probability of a thruster wear-out failure for this worst-case thruster usage.

A. Trajectory and Mission Requirements

This analysis assumes a representative trajectory for the Dawn mission based on a 425-kg xenon load, a 1219-kg spacecraft initial wet mass, and a Mars gravity assist. The solar array output power as a function of mission time is given in Fig. 2. Also shown in this figure is the PPU input power over the mission. For roughly the first 1070 days of the mission the solar array provides more power than can be processed by the IPS. Over this time the IPS is operated at its full power point. After approximately 1070 days the solar array cannot provide sufficient power to operate the IPS at full power. To accommodate the reduction in solar array power the IPS is operated at reduced thrust and power levels. Each ion thruster can be operated over a range of input powers from 481 W to 2318 W. Sixteen separate combinations of propellant flow rates are used to enable thruster operation over this power range. These sixteen flow rate settings are called "Throttle Levels" (TH) and range from TH0 for the lowest power level up to TH15 for the highest power. Each throttle level is then subdivided into seven power levels to provide finer control of the power used by the IPS. This results in a total of 112 unique power levels called mission levels (abbreviated ML) with an average increment of 16 W between levels. All 112 mission levels and the 16 throttle levels are shown in Fig. 3.

Combining the definition of the throttle levels from Fig. 3 with the PPU input power variation from Fig. 2 results in the variation of throttle level with mission time as shown in Fig. 4. The xenon processed as a function of mission time is given in Fig. 5. This figure indicates that the IPS must process approximately 270 kg of xenon to get to Vesta and 395 kg to complete the mission (assuming nominal flow rates). If two thrusters are used for the entire mission, and if it is assumed that the propellant throughput is shared equally between these two thrusters, then each thruster must process 135 kg to get the Dawn spacecraft to Vesta and 198 kg through the end of the Ceres orbital operations.

By comparison, the Extended Life Test (ELT) of the DS1 flight-spare ion thruster demonstrated a propellant throughput capability of 235 kg before the test was suspended [6]. During the ELT the thruster reached its end of life at full power (TH15) after processing 211 kg of xenon, but was still fully functional at all throttle levels from TH0 through TH12 after processing 235 kg. Throttle levels TH13 and TH14 were not tested at any time during the ELT so it is unknown if the thruster would have operated successfully at these throttle levels at the end of the test. A comparison of the xenon processed at each throttle level tested during the ELT with that required per thruster for Dawn under the assumption of the worst-case thruster usage is given in Fig. 6 assuming the two Dawn thrusters share the propellant throughput equally at every throttle level. A summary of the ELT test segments is given in Table 1 [6]. The ELT thruster processed 145 kg of xenon at TH15. Each Dawn thruster must process 95 kg at TH15 under the worst-case mission usage.

II. Service Life Validation

To successfully evaluate the risk of wear-out failures all of the important failure modes must be known. Wear-out failure modes are typically identified by testing. Fortunately, there is an extensive body of life-test experience for ion thruster dating back almost 50 years. A survey of the life-test literature as of 1996 is summarized in Ref. [7]. At that time, based on this literature survey the significant wear-out failure modes for the NSTAR ion thruster, (which was then under development) were identified and are listed in Table 2. Since 1996 ion thrusters of the NSTAR design have successfully completed two long-duration life tests: an 8,200-hr test [8], and a 30,352-hr test [6]. In addition, an NSTAR thruster was operated for over 16,000 hours in space on DS1 [5]. Based on this added extensive test and flight experience the list of significant failure modes was modified as shown in the right most column in Table 2.

Table 2 indicates that the first seven significant wear-out failure modes identified in 1996 are still included in the 2007 list, and that four new items have been added. This would seem to suggest that the 1996 list missed four significant failure modes. The actual situation is not quite that bleak for the following reasons. Item #8, "arcing through the low-voltage propellant isolator," is not actually a damage-accumulation failure mode. Failures by this mode could occur at any time. The Dawn ion thruster design has removed the low-voltage propellant isolator and its functionality has been replaced by the high-voltage propellant isolators. Item #9, "neutralizer clogging at low power," was a known failure mode, but as of 1996 it wasn't believed to be significant to the NSTAR thruster design. An operational change for the Dawn thrusters based on the data from the DS1 Hyper-Extended Mission [5] was made to mitigate this failure mode. Similarly, item #11, "excessive performance degradation or cathode ignition failure due to insert depletion," was also a known failure mode. However, in 1996 this failure mode was not believed to be significant to the NSTAR thruster design and the thruster life testing performed since then has confirmed this. Nevertheless, it was added to the 2007 list in order to make sure sufficient attention is paid to this failure mode to prevent it from becoming significant.

Finally, item #10, "cathode ignition failure due to heater erosion," is the most interesting. Failures by this mode are caused by discharge plasma ions eroding the heater that surrounds the discharge cathode to the point where it is no longer functional. In 1996 this was also a known failure mode. The discharge keeper electrode in the NSTAR thruster design was included specifically to protect the discharge cathode and heater from erosion by ions from the discharge chamber plasma. In the 8,200-hr test, which was performed entirely at the thruster's full power level (TH15), erosion of the keeper electrode was observed. At most 36% of the keeper thickness was eroded during the 8,200-hr test. Extrapolation of this erosion suggested that the thruster could be operated for more than 22,000 hours at full power before the keeper would be eroded away. Once the keeper is eroded away, then ions from the discharge chamber plasma will start eroding the cathode orifice plate and heater ultimately leading to their failure. Furthermore, it was believed that operation at full power is the most stressful condition for the thruster from a wear-out failure perspective and that operation at lower power levels would result in lower component erosion rates. In reality, however, after approximately 10,500 hrs into the ELT the discharge keeper was sufficiently eroded that the discharge cathode heater was fully exposed to the discharge chamber plasma. Of this 10,500 hours only 4,200 hours had been at full power [6]. The key message here is that significant extrapolation from even relatively long tests must be done very carefully. For the Dawn thrusters the discharge chamber keeper material was changed from molybdenum to the more erosion resistant tantalum to slow down the keeper erosion. A healthy keeper electrode will protect the cathode and heater from the discharge ions and mitigate failure modes #6 and #10 in Table 2.

The extended life test of the NSTAR thruster design had no incidents of rogue-hole formation and no unclearable grid shorts (failure modes #1 and #2 in Table 2). In addition, it showed that structural failure of either grid, the

screen grid or the accelerator grid, was far from being the life-limiting wear-out failure mode (failure modes #3 and #7 in Table 2). Independent cathode heater tests showed that thermally cycling the NSTAR cathode heaters (failure mode #5 in Table 2) is not a significant failure mode for the number of heater cycles typically required for a deep-space mission such as Dawn.

This leaves only electron-backstreaming (failure mode #4 in Table 2). The remainder of this paper will deal with the implications of this wear-out failure mode.

III. Electron-Backstreaming

Electron-backstreaming (EBS) is now known to be the life-limiting wear-out failure mode for operation of the Dawn ion thrusters at full power. Interestingly enough it was not apparent until 25,700 hours into the ELT what the life-limiting wear-out failure mode was for the NSTAR thruster design. In the ELT after the thruster had been operated for 25,700 hours and had processed 211 kg of xenon over the throttle profile given in Table 1 it was not possible to prevent EBS at TH15 using the maximum magnitude of the accelerator grid voltage that can be provided by the PPU. However, the thruster was still fully functional at all throttle levels less than or equal to TH12 from this point through the end of the test. There are no simple mitigation approaches that can be used for the Dawn ion thrusters which would not have a major impact on the thruster heritage or the in-flight usage of the thrusters. Therefore, it is critical that this failure mode be well understood in order to assess its impact on the probability of success for the Dawn mission under the assumption of worst-case mission use.

In the analyses that follow, a model of EBS is presented and compared against the EBS data from the ELT. This model is then put in to a probabilistic framework in order to capture the fact that the values of many of the input parameters to the model cannot be specified exactly. The probability of wear-out failures due to EBS is then calculated assuming thruster operation over the representative trajectory discussed above.

The variation in EBS voltage was measured throughout the ELT [6]. These data are reproduced here in Fig. 7, where the magnitude of the accelerator grid voltage at which electron-backstreaming occurs is plotted as a function of run time in the ELT. The vertical dashed lines in this figure indicate the times when the throttle level was changed. Several things are evident from these data. First, there is a general trend toward greater values (in magnitude) of accelerator grid voltage at which electron-backstreaming occurs. This is due to erosion of the accelerator grid apertures by charge-exchange ions. Second, large scale jumps in EBS voltage occur when the throttle level is changed. Finally, when the last TH15 test segment (which took place from run hour 21,306 to 25,706) is compared to the earlier two TH15 test segments, it is clear that the slope of the increase in EBS voltage with run time has increased. Any model of EBS will have to reproduce the behavior displayed in Fig. 7.

Also shown in Fig. 7 are the electron-backstreaming voltages calculated by the CEX2D computer code [9]. These results indicate that the CEX2D code gives a pretty good estimation for the EBS voltage and reproduces many of the key features of the behavior versus run time and throttle level, and in general, tends to somewhat over-predict the magnitude of the EBS voltage, which is conservative. The code, however, misses the increased slope for the third test segment at TH15. This is significant because it suggests that the code does not adequately capture the approach-to-failure that occurred at the end of the third test segment at TH15. In addition, the CEX2D code cannot easily be used in a probabilistic analysis of this failure mode. For this an analytical model is needed.

Therefore, an analytical model consisting of two parts was developed. The first part is an analytical expression for the voltage at which electron-backstreaming occurs for a given set of grid geometry, beamlet current, and applied voltages. The second part is a semi-empirical model of how the accelerator grid geometry changes with time. This semi-empirical model of the accelerator grid geometry as a function of time was used with the CEX2D code to get the calculated values shown in Fig. 7.

A. Model of Electron-Backstreaming

An analytical model for EBS is given by Williams, Goebel and Wilbur in Ref. [10]. This model (which we'll call the WGW model) calculates the accelerator grid voltage, V_a , at which electron-backstreaming occurs for a specified grid geometry and operating state using the following set of equations.

$$V_a = \frac{V_{sp} - \Delta V - V_{dp} B}{1 - B} \quad (1)$$

$$V_{sp} = V_{bp} + T_e \ln \left(\frac{2J_e}{J_b} \sqrt{\frac{V_{dp} - V_{bp}}{T_e}} \left(\frac{\pi m_e}{m_i} \right) \right) \quad (2)$$

$$\Delta V = \frac{J_b}{2\pi \epsilon_0} \sqrt{\frac{m_i}{2e(V_{dp} - V_{sp})}} \left[\frac{1}{2} - \ln \left(\frac{d_b}{d_a} \right) \right] \quad (3)$$

$$B = \frac{d_a}{2\pi l_e} \left[1 - \frac{2t_a}{d_a} \tan^{-1} \left(\frac{d_a}{2t_a} \right) \right] e^{-\frac{t_a}{d_a}} \quad (4)$$

$$l_e = \sqrt{(l_g + t_s)^2 + \frac{d_s^2}{4}} \quad (5)$$

The model is valid for cases where $d_a < l_e$. For the cases examined herein this is not always the case. In general for the Dawn grid geometry at end-of-life it is more typical that d_a is approximately equal to l_e . In addition, the model (as seen in Eq. 4) includes an exponential shielding term that is used to account for the effect of the accelerator grid thickness. Without this term the derivation of the model assumes an infinitely thin accelerator grid. This term was originally used by Kaufman to better explain electron-backstreaming data for electrodes of finite thickness. Therefore, the WGW model is also essentially a semi-empirical one whose range of applicability is marginal for our intended use. Nevertheless, it is the best analytical model available and, as will be shown later, it appears to give results at least as good as numerical simulations of the grid system EBS behavior.

The ratio J_e / J_b represents the fraction of the beamlet current at which electron-backstreaming is said to occur. For the analyses presented herein a value of 10% was used. This value was selected based on the following rationale. Measurements of electron-backstreaming during the Dawn thruster acceptance tests were based on a measured increase in beam current of 1 to 2 mA. At full power (TH15) the beam current is 1760 mA and the peak beamlet current is approximately 0.27 mA/hole. The beamlet current profile (shown later in Fig. 10) is approximately constant at the peak value out to a radius of about 1 cm. A 1-cm radius circle contains approximately 65 holes. If each of these holes has a beamlet current of 0.27 mA, then the total beam current from this region is 17.6 mA, and 10% of this is 1.8 mA, which meets our criteria of being between 1 and 2 mA. It is assumed that there is no electron-backstreaming outside of this 1-cm radius region. Therefore, an electron-backstreaming fraction of 10% over a 1-cm radius circle centered on the location of the peak beamlet currents will result in an observable electron-backstreaming current. Fortunately, the EBS results are not very sensitive to the assumed value of this ratio. For example, it will be shown later that for thruster operation at full power (TH15) the peak in the failure distribution curve for EBS occurs at a propellant throughput of 189 kg (for a maximum $|V_a| = 250$ V). Decreasing the value of J_e / J_b by an order of magnitude from 0.10 to 0.01 changes the peak in the failure distribution curve by about 1% (from 189 kg to 187 kg). Similarly, increasing J_e / J_b by an order of magnitude from 0.10 to 1.00 changes the peak in the failure distribution by about 5% (from 189 to 198).

To use the WGW model to reproduce the behavior in Fig. 7 we need to be able to specify the values of ten input parameters as a function of time over the full throttle range of the thruster (or at a minimum at the throttle levels TH0, TH5, TH8, TH12 and TH15 which were used in the ELT). These parameters are the accelerator grid hole diameter (d_a), the beamlet diameter (d_b), the screen grid hole diameter (d_s), the beamlet current (J_b), the grid gap (l_g), the electron temperature (T_e), the accelerator grid thickness (t_a), the screen grid thickness (t_s), the beam plasma potential (V_{bp}), and the discharge plasma potential (V_{dp}).

We will take the screen grid hole diameter to be constant since no significant changes in the screen grid hole diameters were measured after the ELT [6]. The screen grid thickness, in the worst case, had decreased to approximately 60% of its original thickness over the course of the ELT [6]. In the analysis that follows this change in thickness is approximated as a linear function of the propellant throughput. A more sophisticated screen grid erosion model could be used, but for the purposes of examining accelerator grid EBS this was considered unnecessary. This leaves us with nine parameters that must be specified either as a function of the throttle level (d_b , J_b , l_g , T_e , V_{bp} , V_{dp}) or as a function of run time (d_a , t_a and t_s).

The beam plasma potential was measured in the LDT and was found to vary non-monotonically from 3 V to 5 V (relative to facility ground) over the full throttle range [8]. In addition, the coupling voltage as measured in the ELT was also found to vary non-monotonically over the full throttle range with values from -10 V to -16 V. The beam plasma voltage is the beam plasma potential relative to ground minus the coupling voltage. The beam plasma potential measured in the LDT of 4 V, and the measured coupling voltage of -11 V were used to get $V_{bp} = 4 \text{ V} - (-11 \text{ V}) = 15 \text{ V}$. In the probabilistic analyses V_{bp} is assumed to uncertain by +/- 5V.

The discharge plasma voltage, V_{dp} , is simply the applied beam power supply voltage at each throttle level. The electron temperature, T_e , was assumed to be 1.8 eV at all throttle levels based on the data in Ref. [11]. In the probabilistic analyses T_e is assumed to uncertain by +/- 1 eV.

Initially, the accelerator grid thickness was fixed at its beginning-of-life value (0.508 mm) for the entire service life of the thruster. This was subsequently modified to allow thinning of the accelerator grid near end-of-life in order to get better agreement with the approach-to-failure data given in Fig. 7. We now have four parameters left to specify, the beamlet current, the beamlet diameter, the grid gap, and the accelerator grid hole diameter.

B. Ion Beamlet Characteristics

The beamlet current is determined from Faraday probe traces taken approximately 2.5 cm downstream of the thruster centerline. Faraday probe traces were taken for all three Dawn thrusters during formal acceptance testing at the following throttle levels: TH0, TH3, TH6, TH9, TH12 and TH15. Similar traces were taken years earlier with the LDT and ETL thrusters. The Faraday probe trace yields current density as a function of radial position in a plane normal to the thruster centerline. The WGW EBS model, however, requires a knowledge of the current through each beamlet, that is, through each pair of screen-accelerator grid apertures.

The procedure illustrated in Fig. 8 is used to extract the beamlet currents from the Faraday probe data. As suggested in this figure, the typical Faraday probe trace is both somewhat asymmetric and the peak current density is generally observed to be off the geometric centerline of the thruster. The analysis begins by first shifting the centerline to maximize the right-left symmetry of the trace. The right and left sides are then averaged to produce a perfectly symmetrical beam current density profile. This profile is then input to computer program which calculates the beamlet current required through each of the 15,000 grid apertures in order to produce the input Faraday probe trace. The program accounts for the curvature of the grids and the variation in beamlet divergence as a function of beamlet current. It assumes a uniform current density in each beamlet. The beamlet divergence angles were obtained from the CEX2D ion optics computer model and are plotted in Fig. 9. The end result of this process is given in Fig. 10 for Dawn thruster FT3 operating at TH15. This figure indicates a peak beamlet current of about 0.27 mA.

The same process was used to analyze the Faraday probe traces taken on the LDT thruster and the two DS1 flight thrusters (DS1-FT1 flew on DS1, and DS1-FT2 became the ELT thruster). These results, shown in Fig. 11 for thruster operation at TH15, indicate that the maximum beamlet current varies from 0.27 mA to 0.30 mA for thrusters with identical magnetic circuits operated in the same way. Similar beamlet profiles for all three Dawn thrusters are given in Figs. 12-14 for FT1, FT2 and FT3, respectively. These data indicate that the maximum beamlet current varies from 0.27 mA to 0.33 mA (i.e., 0.30 mA + 10%) for the Dawn thrusters with FT002 having the highest maximum beamlet current. Continuing this process over the full throttle range yields the results shown in Fig. 15 where the maximum beamlet currents are plotted as a function of throttle level for all three Dawn thrusters along with the LDT and ELT thrusters. The measured EBS voltages are plotted against the peak beamlet currents in Fig. 16. This figure indicates that increasing peak beamlet currents result in greater measured electron-backstreaming voltages and the data is consistent between all three thrusters.

An important parameter in the WGW model is the diameter of the beamlets. Three different models of the variation of the beamlet diameters with beamlet current were investigated. These models included unpublished data on directly measured beamlet diameters; no variation (i.e., beamlet diameter is independent of the beamlet current); and beamlet diameters calculated by the CEX2D code. Use of beamlet diameters calculated by the CEX2D code resulted in the best agreement with the data and, therefore, the CEX2D results were used in the subsequent analyses with one modification. The values used corresponded to the beamlet diameters at the downstream plane of the accelerator grid aperture and are given in Fig. 17. There is no a priori guarantee that this location corresponds to the location of the saddle point voltage. The best agreement was obtained by multiplying the CEX2D beamlet diameters by 0.9. The resulting beamlet diameters versus beam current (i.e., throttle level) are given in Fig. 18 for both a nominal Dawn thruster and the ELT thruster.

The hot grid gap, l_g , is another important parameter required by the WGW model. Four independent approaches to determining the hot grid gap were investigated. First, finite element modeling of the grid system predicts a hot

grid gap at TH15 of 480 microns [12]. Second, the post test cold grid gap for the ELT thruster was 490 microns [6] suggesting the grid system may have taken on a permanent set at this gap. Third, beamlet deflection measurements made at TH15, TH10, and TH4 were used to back out the hot grid gap at these throttle levels [13]. This process suggested a hot grid gap of 480 microns at TH15. Fourth, direct measurements of the hot grid gap have been made on a functional model thruster and relatively new grids at TH15, TH8 and TH0 [14]. These measurements indicate a much smaller hot grid gap of only 300 microns at TH15. Comparison of the grid gaps from Refs. 13 and 14 is given over the throttle range in Fig. 19. Clearly there is a significant difference in the values of the gaps determined by these different techniques. To be conservative the directly measured values were used in the subsequent analyses. The analyses assume that the hot grid gaps don't change as a function of propellant throughput.

Using the hot grid gaps from Fig. 19 and the beginning-of-life grid geometry in WGW model gives the solid line shown in Fig. 16. These results agree well with the measured data. This formulation produces approximately the right values with approximately the right slope. Other calculations made with the CEX2D code indicate that the beamlet diameters don't change significantly as the accelerator grid apertures enlarge due to erosion.

C. Accelerator Grid Hole-Wall Erosion

The final key parameter required by the WGW model is the accelerator grid hole diameter. Determination of the correct value of this parameter as a function of time is not straight forward. This difficulty results primarily from the fact that the hole diameter itself is not well defined. At the beginning-of-life the hole geometry is cusped-shaped, as shown in Fig. 20, due to the chemical etching process used to form the holes. The end-of-life hole geometry is also shown in Fig. 20 [6]. The minimum hole diameter has moved upstream almost 100 microns and the hole now has a distinctive chamfered shape at the downstream surface. The time-evolution of the hole geometry from the BOL shape to the EOL shape is assumed to follow three phases. The first phase removes the cusps formed from the chemical etching process creating holes with an approximately cylindrical shape. The second phase maintains the cylindrical hole wall shape and increases the diameter to the final minimum hole diameter. The third phase chamfers the downstream end of the hole. Chamfering at the upstream end is ignored.

Measurements of the minimum accelerator grid hole diameter in the center of the grid are given in Fig. 21 as a function of time in the ELT. Also shown in this figure is the prediction of accelerator grid erosion model that follows the three erosion phases discussed above. Note that during the "chamfering" phase the minimum hole diameter does not change. In this phase, only the downstream end of the accelerator grid aperture is enlarged. During the ELT it was known that the minimum accelerator grid hole diameter in the center of the thruster stopped enlarging after about 12,000 hrs of operation. The photographic measurement technique that determined this, however, could not detect the chamfering of the holes. It was also known that the magnitude of the electron-backstreaming voltage continued to increase. How to reconcile of these facts remained a mystery until the post-test examination of the accelerator grid revealed the significant chamfering at the downstream end of the apertures. It is interesting to note that this change in erosion geometry was not evident in the 8,200-hr LDT. In the ELT it took more than 12,000 hours of operation to identify this erosion pattern which is a key feature in the wear-out failure of the accelerator grid by electron-backstreaming.

The notional erosion model consisting of the three phases discussed above is made quantitative by using the results from the ELT. As indicated in Table 1 the ELT was operated in seven test segments in the following order of throttle levels: TH12, TH15, TH8, TH15, TH0, TH15, and TH5. The total mass removed from the accelerator hole wall, M_{AHW} , is simply given by:

$$M_{AHW} = \dot{m}_{TH12}T_1 + \dot{m}_{TH15}T_2 + \dot{m}_{TH8}T_3 + \dot{m}_{TH15}T_4 + \dot{m}_{TH0}T_5 + \dot{m}_{TH15}T_6 + \dot{m}_{TH5}T_7 \quad (8)$$

where T_1 through T_7 are the durations spent at each test segment as given in Table 1 and \dot{m}_{THxx} is the accelerator hole wall erosion rate at throttle level THxx. This formula can be rearranged as:

$$M_{AHW} = \dot{m}_{TH15} \left[T_2 + T_4 + T_6 + \frac{\dot{m}_{TH12}}{\dot{m}_{TH15}} T_1 + \frac{\dot{m}_{TH8}}{\dot{m}_{TH15}} T_3 + \frac{\dot{m}_{TH0}}{\dot{m}_{TH15}} T_5 + \frac{\dot{m}_{TH5}}{\dot{m}_{TH15}} T_7 \right] \quad (9)$$

The ratios $\frac{\dot{m}_{THxx}}{\dot{m}_{TH15}}$ are obtained from the CEX2D computer code. These ratios, which were obtained using the value

for \dot{m}_{TH15} at an accelerator grid voltage of -180 V, are plotted in Fig. 22 for three values of the accelerator grid voltage: -180 V, -200 V and -250 V. These data indicate that the ratio of the accelerator grid hole wall at any throttle level compared to that at full power (TH15) is not sensitive to the accelerator grid voltage. The 3rd order polynomial curve fit shown on this figure was generated to facilitate interpolation to other throttle levels.

The final step is to adjust the value for \dot{m}_{TH15} until the above formula produces the measured value for the centerline accelerator grid hole mass loss of 2.69 mg [6]. This requires that $\dot{m}_{TH15} = 0.141 \text{ mg}/\text{hr}$. With this value, the erosion model now enables the mass loss from the centerline accelerator grid hole to be calculated at any time for any combination of throttle levels. The corresponding grid aperture geometry can then be determined using the assumption of the three phases of erosion described above.

D. Accelerator Grid Pits & Grooves Erosion

The photograph in Fig. 23 shows the characteristic “pits & grooves” erosion pattern on the downstream side of the accelerator grid. This erosion can contribute to the failure of the accelerator system in three ways. First, it is clear from this picture that in the “pits” locations the erosion has proceeded completely through the grid. If the erosion in the “grooves” regions between the pits also proceeds completely through the grid, then the grid will fail structurally. Second, when the erosion in the pits regions penetrates the grid, erosion on the *upstream* side of the accelerator grid will then occur. Some of the material eroded from the upstream surface will get deposited on the downstream surface of the screen grid. This material could subsequently flake off and electrically short the grids. Finally, the pits & grooves erosion pattern could intersect the enlarged grid apertures. This is clearly what has happened in the photograph in Fig. 23. At this time the geometry of the grid changes significantly and relatively rapidly. Only small islands of the original accelerator grid thickness are visible in Fig. 23. The rest of the grid is thinner which contributes to the onset of electron-backstreaming.

Erosion in the pits & grooves pattern is handled with the same methodology used for the grid-hole erosion. The total mass removed from the pits & grooves region around each hole is given by,

$$M_{pg} = \dot{m}'_{TH12}T_1 + \dot{m}'_{TH15}T_2 + \dot{m}'_{TH8}T_3 + \dot{m}''_{TH15}T_4 + \dot{m}_{TH0}T_5 + \dot{m}''_{TH15}T_6 + \dot{m}''_{TH5}T_7 \quad (10)$$

where the parameter \dot{m}'_{THxx} indicates the mass removal rate from the pits & grooves region at throttle level $THxx$ at the beginning of life accelerator grid voltages. The parameter \dot{m}''_{THxx} indicates the mass removal rate at end of life accelerator grid voltage of -250 V. This equation is then rewritten in the form,

$$M_{pg} = \dot{m}''_{TH15} \left(\frac{\dot{m}'_{TH12}}{\dot{m}''_{TH15}}T_1 + \frac{\dot{m}'_{TH15}}{\dot{m}''_{TH15}}T_2 + \frac{\dot{m}'_{TH8}}{\dot{m}''_{TH15}}T_3 + T_4 + \frac{\dot{m}'_{TH0}}{\dot{m}''_{TH15}}T_5 + T_6 + \frac{\dot{m}''_{TH5}}{\dot{m}''_{TH15}}T_7 \right) \quad (11)$$

The ratios $\frac{\dot{m}'_{THxx}}{\dot{m}''_{TH15}}$ are calculated using the CEX2D code. It may seem more appropriate to use the 3-dimensional

CEX3D code for these calculations [15], but since we're interested only in the ratios of the erosion rates, the 2-dimensional CEX2D code should be adequate. The resulting normalized ratios are given in Fig. 24. Also included in this figure are the normalized erosion rate ratios for the hole-wall erosion used in Eq. (9) and reproduced from Fig. 22. The relative erosion rates given in Fig. 24 were fit to cubic polynomials to enable interpolation to other throttle levels. These curve fits are all in the form:

$$\text{Mass of Material Eroded: } M = a_o + a_1TH_{xx} + a_2TH_{xx}^2 + a_3TH_{xx}^3$$

where the coefficients a_0 through a_3 are given in Table 5. These curve fits were then used in Eqs. (9) and (11) and the values of \dot{m}_{TH15} and \dot{m}''_{TH15} are selected so that the results matched the measured masses of material eroded in the hole wall (2.69 mg), and pits & grooves (3.40 mg), respectively. The values for \dot{m}_{TH15} and \dot{m}''_{TH15} are also given in Table 5.

E. Deterministic Analysis Results

With this formulation we can now calculate the amount of material eroded from the hole walls or in the pits & grooves pattern as a function of time for those holes where the beamlet current is a maximum. This can be done for any combination of throttle levels in any order. For the throttle levels that correspond to the representative trajectory of Fig. 4 the estimated material removed from the accelerator hole wall as a function of propellant throughput processed per thruster is given in Fig. 25. There are four curves given in this figure. The one labeled “One thruster” assumes that a single thruster is used for the entire mission. The curves labeled, “Two thrusters share equally” and “Three thrusters share equally,” assume that two or three thrusters are used for the mission and that the propellant throughput is shared equally among the thrusters at every throttle level. Also shown in this figure is a curve that corresponds to the ELT. The ELT curve rises more slowly than those corresponding to the Dawn trajectories because the ELT thruster was operated at throttle levels less than TH15 earlier (i.e., at lower propellant throughputs) than is required by the representative Dawn trajectory. The changes in slopes of all the curves correspond to operation at different throttle levels.

The ELT thruster had reached its end-of-life for operation at full power prior to the end of the test. This is estimated to have occurred after approximately 2.58 mg of material had been eroded per hole from the hole walls. If a single thruster is used for the entire mission, it will result in much larger values of material eroded per hole. As we will see in the subsequent section, there is a 100% probability that a single thruster will wearout if it is attempted to be used for the entire mission.

A similar set of curves is given in Fig. 26 for the pits & grooves erosion. The three Dawn-trajectory related curves in this figure are seen to start out with a slightly steeper slope than the ELT curve up to a propellant throughput of about 70 kg. This is a result of starting the Dawn thrusters out with an accelerator grid voltage of -200 V instead of the -180 V used in the ELT at full power. The slope change in the three Dawn-trajectory related curves at about 70-kg throughput corresponds to changing the accelerator grid voltage from -200 V to -275 V to prevent electron-backstreaming as the grid wears. For the ELT thruster the accelerator grid voltage was changed from -180 V to -250 V after the thruster had processed 88 kg of xenon (with the exception of the TH0 test segment which was run with an accelerator grid voltage of -150 V).

F. Calculated EBS vs Time in the ELT

Close examination of the data in Fig. 7 indicates that in the third test segment at TH15, which covers the run times from 21,306 hours to 25,706 hrs, there is a clear change in slope that occurred at approximately 23,600 hours. To account for this in the EBS model, it was assumed that effective thinning of the accelerator grid began at this time. Post-test measurements of the accelerator grid indicated a reduction in grid thickness around the holes near the thruster centerline from the original thickness of 508 microns to approximately 450 microns [6]. The run time of 23,600 hours at which this thinning is assumed to begin corresponds to a maximum estimated mass removed per hole from the hole wall of 2.28 mg. The final maximum hole-wall mass removed per hole from the holes near the thruster centerline was 2.69 mg as determined by post-test measurements [6]. The grid erosion model described above estimates a maximum mass removed per hole of 2.77 mg over the ELT. This corresponds to an over prediction of the maximum hole-wall mass removed of only 3%. The grid thinning occurs at this time due to an intersection of the pits & grooves erosion pattern on the downstream side of the grid with the hole-wall erosion pattern as shown in Fig. 23. Thinning of the accelerator grid is assumed to vary linearly with the amount of hole-wall mass removed over the range from 2.28 mg to 2.77 mg as indicated in Fig. 27.

During the ELT the grid system had reached its end-of-life at TH15 after 25,706 hours of operating time corresponding to a total propellant throughput of 211 kg of xenon. The grid erosion model estimates that at this time the maximum hole-wall mass loss was 2.58 mg. Note the measured EBS data in Fig. 7 at 25,706 hours do not exceed the 250-V capability of accelerator power supply suggesting that the grid system was still operational. As the end-of-life was approached, measurements of the EBS voltage were recorded approximately every 25 to 50 hours until electron-backstreaming could not be prevented. Only the data in which a successful EBS measurement could be made were recorded. The highest recorded value was 242 V, which is still 8 V below the capability of the

accelerator power supply. This suggests that the onset of EBS voltages greater than the power supply capability is quite rapid (relative to the time-scale of normal thruster operation) and can correspond to EBS voltage changes of greater than 8 V.

Using the semi-empirical formulation described above for the erosion of the accelerator-hole walls together with the WGW model enables the electron-backstreaming voltage to be calculated as a function of time in the ELT. To do this the parameter values listed in Tables 3 and 4 were used and the results are given in Fig. 28. The model gives reasonably good agreement with the measured EBS data. It appears to give approximately the right slopes and reproduces the changes with throttle level. For the last ELT test segment at TH15, the WGW model under-predicts the EBS voltage at failure by up to 31 V. For this reason and to add a small amount of conservatism a fixed 35 V is added to the WGW model to determine the EBS voltage near end-of-life in the probabilistic analyses that follow.

G. Probabilistic Failure Analysis (PFA) Model

The EBS and wear models presented above are deterministic. In reality, of course, not all of the input parameters required by these models can be specified exactly. This uncertainty in the input parameters can be handled by putting the analysis into a probabilistic framework in which the key input parameters are allowed to vary over specified ranges of values. In general, the values could have specified distributions – if known – over these ranges. For the analyses presented below all of the parameter distributions are assumed to be uniform over the specified ranges. The key parameters and their ranges of allowed variation are given in Table 7. The ranges in this table were selected to capture the uncertainty to which these parameter can be specified. It is not expected in every case that each of these parameters actually has this range of variability. The ranges in Table 7 include our lack of knowledge regarding how to specify these parameters exactly.

The range in sputter erosion rates was selected as follows. The 8,200-hr Life Demonstration Test (LDT) indicated a peak sputter erosion rate for the accelerator grid hole walls of 0.124 mg/khr at TH15. The ELT results indicated an average rate of 0.146 mg/khr at TH15. Using the ELT as the “nominal” rate, the measured LDT rate is 15% less than this. The erosion model presented above also calculates that the pits & grooves erosion in the LDT is 44% of the total accelerator grid erosion. This agrees well with the 43% estimate in Ref. [8] for the pits & grooves erosion fraction. The erosion rates were assumed to vary by +/-15% from the ELT values.

The propellant flow rate uncertainty of +/-3% is simply the requirement for the propellant feed system which is met by the flight system. The beamlet current uncertainty of +/-10% captures the range of peak beamlet currents at TH15 observed on the five flight thrusters that have been built and tested (2 for DS1 and 3 for Dawn), as well as the engineering model thruster used in the LDT. The beamlet diameter uncertainty was assumed to be the same as the beamlet current uncertainty. The uncertainty in the width of the pits & grooves erosion pattern was taken from measurements made on the LDT thruster [8]. The beam plasma potential uncertainty of +/-5 V represents an uncertainty of 33%.

The PFA process uses these parameter ranges in a Monte Carlo simulation. The value for each parameter in Table 7 is selected at random from within the specified range. The model then calculates the amount of grid material removed as a function of time in increments of 100 hours. For each increment of time the electron-backstreaming voltage is calculated using the WGW model presented above. If the EBS voltage is greater than the maximum capability of the accelerator power supply (which is 275 V for Dawn and 250 V for NSTAR/DS1), or the pits & grooves pattern has eroded completely through the grid, or the pits & grooves pattern has intersected with the chamfered accelerator grid apertures, then the grid is said to have reached its end-of-life. This process is repeated typically 25,000 times to determine the failure probability as a function of run time (or propellant throughput).

Full Power Operation Only: The results of PFA process are shown in Fig. 29 for the ELT thruster operating at TH15. This figure gives the calculated failure distribution as a function of propellant throughput – that is, how many times did a calculated failure occur at each propellant throughput. The most probable throughput at which failure will occur corresponds to the peak in the failure distribution. For Fig. 29 this is at a throughput of 197 kg. The width of the distribution is determined by the ranges of the key parameters specified in Table 7. With these specified ranges, Fig. 29 indicates that there is one chance in a thousand that that the grids could fail due to electron-backstreaming after processing only 128 kg. Similarly, there is some chance that the failure won't occur until after the thruster has processed 250 kg. From a mission success standpoint, we are concerned with the tail of the distribution on the left-hand side. The calculated failure distribution fits relatively well to a Gaussian distribution as indicated in this figure with a standard deviation of 23 kg. This is significant since the tail of a Gaussian distribution falls of quite rapidly with distance from the peak.

Integrating the curve in Fig. 29 up to any specified throughput yields a curve of the total failure probability as a function of throughput as shown in Fig. 30. This figure indicates that there is a less than 1% probability that the grids will fail due to EBS after processing 140 kg of xenon at full power. The 50% failure probability in Fig. 30 corresponds to the peak of the failure distribution in Fig. 29.

ELT Simulation: The PFA model of accelerator grid wearout was used to simulate the ELT results. The model was run over the throttling profile used in the ELT as given in Table 1. The only exception to this was that if the thruster had not failed by the time it completed all of the ELT test segments, the simulated thruster operation was continued at TH5 until the thruster did fail. The results of this process are shown in Figs. 31 and 32. The failure distribution in Fig. 31 actually suggests two different distributions. The first distribution is associated with operation at full power. The second distribution is for operation at lower power levels, with most of this being at TH5. This change in distributions is what gives the unusual shape to the failure probability curve in Fig. 32. This curve indicates that there was approximately a 39% chance that the ELT thruster would fail due to EBS at the end of the last test segment at TH15. This is consistent with the actual test since the ELT thruster did fail due to EBS at the end of this test segment. After this failure, the ELT was continued for another 4646 hours at TH5 and processed an additional 24.3 kg of xenon at this throttle level. The test was terminated after processing a total of 235 kg of xenon (corresponding to a calculated failure probability of 41%). If the test had been extended further at TH5, the PFA indicates that the 50% failure probability would have occurred at a throughput of roughly 260 kg. The peak of the second failure distribution in Fig. 31 occurs at a throughput of approximately 300 kg, so it is likely that the ELT thruster could have processed significantly more propellant than the 235 kg actually demonstrated in the test – at least from the standpoint of accelerator grid erosion. In any case it is clear that the predictions of probabilistic formulation of the electron-backstreaming model agree well with the results from the ELT.

One Thruster for the Entire Mission: The PFA was used to determine the probability that a single ion thruster could perform the entire Dawn mission. The trajectory illustrated in Fig. 2 was used in the PFA to determine the thruster wearout probability as a function of propellant processed. To complete the entire Dawn mission with a single thruster requires it to process a total of approximately 395 kg of xenon. The results of the PFA are given in Fig. 33. This figure indicates a 50% probability of thruster failure after a throughput of 218 kg and 100% probability of failure at approximately 270 kg. Clearly, a single thruster cannot be expected to perform the entire Dawn mission.

Two Thrusters for the Entire Mission: The PFA model was run assuming two nominal ion thrusters are operated for the entire mission and that the propellant throughput is shared equally between them at every throttle level. The use of two thrusters for the entire mission represents the worst-case mission use. The model indicated no wearout failures. However, one of the thrusters (FT2) actually has a peak beamlet current at TH15 that is about 15% higher than the nominal value assumed above. Therefore, the PFA was re-run with the peak beamlet currents increased by 15%. The corresponding hole-wall erosion rates and pits & grooves erosion rates were also increased by 15%. To be conservative these increases in beamlet currents and erosion rates were applied over the full throttle range even though the measured peak beamlet currents for FT2 are only higher than the nominal curve fit values at TH15. The effect of the peak beamlet current is shown in Fig. 34 where the failure risk is plotted for operation at TH15 only, with three values of the peak beamlet current: nominal, +10%, and +20%. These results are then cross-plotted in Fig. 35. The results in Fig. 35 indicate that the propellant throughput based on accelerator grid erosion is a linear function of the beamlet current with a slope of -2.5 kg/%. That is for every percent increase in the peak beamlet current, the propellant throughput capability at TH15 is reduced by 2.5 kg. A 10% increase in the peak beamlet current would decrease the throughput capability by a non-negligible 25 kg.

With 15% higher beamlet currents (corresponding to the use of thruster FT2) the PFA indicated that there is a 5.5% probability that the thruster will fail under the worst-case mission use constraint before processing the required 197 kg of xenon. The calculated failure probability as a function of propellant throughput is given in Fig. 36. This figure shows that there is less than 1% probability of failure due to accelerator grid erosion up to a propellant throughput of 178 kg and a 5.5% probability that it will fail at 197 kg. Failure of this thruster, however, doesn't necessarily mean that the mission has failed. It may be possible for the mission to be completed using the remaining thruster. In this case the remaining thruster would have to process the propellant that wasn't processed by the thruster that wore out, as well as processing all of the propellant that it is responsible for. In general, for the mission to be accomplished with just two thrusters, each thruster has to process approximately 197 kg of xenon. In this case, if one of these thrusters fails after processing 178 kg, then the remaining thruster would have to process 197 kg plus

the 20 kg not processed by the failed thruster for a total of 217 kg. Since this is still less than the 235-kg xenon throughput demonstrated in the ELT, there is some reasonable expectation that this may be possible.

The PFA was re-run for the case where two thrusters would share equally the propellant throughput through 178 kg each and then one thruster would complete the mission. This remaining thruster was assumed to have beamlet currents and erosion rates that were 5% above the nominal, i.e., this would correspond to the characteristics of FT1. The results of the PFA are given in Fig. 37 where it is shown that there is a 3.2% probability of the thruster failing due to wearout of the accelerator grid. Therefore, the probability of mission success is calculated as follows. There is 99% probability that the first thruster (FT2) will successfully process 176 kg of xenon. Of the approximately 1% of the cases where the thruster fails after processing 176 kg of xenon (or more), there is a 97% probability that the second thruster can successfully complete the mission. To be conservative we'll assume that all 5.5% of the failure in Fig. 36 occurred at 176 kg. The probability of mission success, from the perspective of accelerator grid life, is $0.945 + 0.055 \times 0.97 = 0.998$, under the assumption that the mission is performed with just two ion thrusters and these two thrusters are the ones with the highest peak beamlet currents (i.e., the worst ones).

IV. Conclusion

The ion propulsion system for Dawn is capable of performing the entire mission, which requires processing approximately 400 kg of xenon, with just two of the three on-board ion thrusters. The failure of one thruster right at the start of the mission represents the worst-case mission use for the remaining two thrusters. Assessment of the wear-out failure risk for these remaining two thrusters requires that all of the significant wear-out failure modes be known. The substantial body of life-test experience accumulated over nearly 50 years of ion thruster development in general and over 13 years of ground and flight test experience with the thruster design for Dawn give high confidence that all of the important wear-out failure modes are known. On the basis of this experience, which most significantly includes a 30,352-hr life test, it is known that the life-limiting wear-out failure mode for the Dawn ion thrusters is electron-backstreaming due to erosion of the accelerator grid by charge-exchange ions. Most significantly the 30,352-hr life test actually tested the thruster to failure at full power. This portion of the test provides essential information about the physics of the failure mechanism. A key feature of this is the understanding of how the accelerator grid geometry changes with time as it erodes. Note, extrapolation from the results of an earlier, fairly long life test of 8,200 hours, did not capture the essential details necessary to properly model this failure mechanism.

A semi-empirical model of the accelerator grid erosion geometry as a function of time is developed based on the information from the 30,352-hr life test. This erosion model is used in an analytical model which calculates the electron-backstreaming voltage as a function of the grid geometry, ion current, and applied voltage. The resulting combined model gives predictions of the electron-backstreaming voltage as a function of time that agree well with the values measured in the 30,352-hr life test. This combined analytical model is used in a probabilistic framework to assess the wear-out failure risk for the worst-case mission use of the ion thrusters for the Dawn mission. The probabilistic analyses indicate that the wear-out failure risk is less than 1% if the worst two Dawn ion thrusters have to perform the entire mission.

Acknowledgments

This research was carried out, in part, at the Jet Propulsion Laboratory, California Institute of Technology, under a contract with the National Aeronautics and Space Administration.

References

1. Rayman, M. D., Fraschetti, T. C., Raymond, C. A., Russell, C. T., Dawn: A Mission in Development for Exploration of Main Belt Asteroids Vesta and Ceres," *Acta Astronautica* 58 (2006 605-616).
2. Brophy, J. R., et al., "Ion Propulsion System (NSTAR) DS1 Technology Validation Report," JPL Publication 00-10, October 2000.
3. Rayman, M. D., "The Successful Conclusion of the Deep Space 1 Mission: Important Results Without a Flashy Title," *Space Technology* 23, Nos. 2-3, p. 185-196 (2003).
4. Rayman, M. D. and Varghese, P., "The Deep Space 1 Extended Mission," *Acta Astronautica* 48, No. 5-12, pp. 693-705 (2001).

5. Brophy, J. R., Brinza, D. E., Polk, J. E., Henry, M. D., and Sengupta, A., "The DS1 Hyper-Extended Mission, AIAA-2002-3673, presented at the 2002 Joint Propulsion Conference, Indianapolis, IN, July 7-10, 2002.
6. Sengupta, A, et al., "The 30,000-hour Extended-Life Test of the Deep Space 1 Flight Spare Ion Thruster," NASA/TP 2004-213391, March 2005.
7. Brophy, J. R., Polk, J. E., and Rawlin, V. K., "Ion Engine Service Life Validation by Analysis and Testing," AIAA-96-2715, presented at the 32nd Joint Propulsion Conference, Lake Buena Vista, FL, 1996.
8. Polk, J. E., "An Overview of the Results from an 8200 Hour Wear Test of the NSTAR Ion Thruster," AIAA-99-2446, presented at the 35th AIAA/ASME/SAE/ASEE Joint Propulsion Conference, 20-24 June 1999, Los Angeles, CA.
9. Brophy, J. R., Katz, I., Polk, J. E., and Anderson, J. R., "Numerical Simulations of Ion Thruster Accelerator Grid Erosion," AIAA 2002-4261, presented at the 38th AIAA/ASME/SAE/ASEE Joint Propulsion Conference & Exhibit, 7-10 July 2002, Indianapolis, Indiana
10. Williams, J. D., Goebel, D. M., and Wilbur, P. J., "Analytical Model of Electron Backstreaming for Ion Thrusters," AIAA-2003-4560, presented at the 39th AIAA/ASME/SAE/ASEE Joint Propulsion Conference, 20-23 July 2003, Huntsville, AL.
11. Brinza, et al., "An Overview of Results from the Ion Diagnostics Sensors Flown on DS1, AIAA 2001-0966, presented at the 39th AIAA Aerospace Sciences Meeting & Exhibit January 8-11, 2001 Reno, NV.
12. Shchedrin, Dmitry, "ION Thruster Grid," Prepared under CWO 0090, Swales Report Number: 28 June 2004.
13. Haag, Thomas, "Translation Optics for 30 cm Ion Engine Thrust Vector Control, "IEPC-01-116, presented at the 27th International Electric Propulsion Conference, Pasadena, CA, 15-19 October, 2001.
14. Diaz, E. M., and Soulas, G. C., "Grid Gap Measurement for an NSTAR Ion Thruster," NASA/TM—2006-214249, IEPC—2005—244, presented at the 29th International Electric Propulsion Conference, Princeton, New Jersey, October 31–November 4, 2005.
15. Anderson, J. R., Katz, I., and Goebel, D., " Numerical Simulation of Two-Grid Ion Optics Using a 3D Code," AIAA-2004-3782, presented at the 40th AIAA/ASME/SAE/ASEE Joint Propulsion Conference and Exhibit, July 11 – 14, 2004, Fort Lauderdale, Florida.

Table 1. Summary of ELT Test Segments.

| Test Segment | 1 | 2 | 3 | 4 | 5 | 6 | 7 |
|----------------------------|------|-------|--------|--------|--------|--------|--------|
| Throttle Level | TH12 | TH15 | TH8 | TH15 | TH0 | TH15 | TH0 |
| Power Level (kW) | 2.0 | 2.3 | 1.5 | 2.3 | 0.5 | 2.3 | 1.1 |
| Duration (hrs) | 447 | 4246 | 5758 | 5166 | 5689 | 4400 | 4646 |
| Xe Processed (kg) | 3.9 | 44.0 | 39.7 | 54.3 | 22.4 | 46.5 | 24.5 |
| Cumulative Throughput (kg) | 3.9 | 47.9 | 87.6 | 141.9 | 164.3 | 210.8 | 235.3 |
| Cumulative Duration (hrs) | 447 | 4,693 | 10,451 | 15,617 | 21,306 | 25,706 | 30,352 |

Table 2. Known Significant NSTAR Ion Thruster Wear-out Failure Modes.

| Item | As of 1996 | As of 2007 |
|------|---|---|
| 1. | Accelerator grid failure due to rogue-hole formation | Accelerator grid failure due to rogue-hole formation |
| 2. | Accelerator system failure due to unclearable grid-to-grid shorts | Accelerator system failure due to unclearable grid-to-grid shorts |
| 3. | Structural failure of the accelerator grid due to erosion by charge-exchange ions | Structural failure of the accelerator grid due to erosion by charge-exchange ions |
| 4. | Thruster failure due to electron-backstreaming resulting from aperture enlargement by charge-exchange ion erosion | Thruster failure due to electron-backstreaming resulting from aperture enlargement by charge-exchange ion erosion |
| 5. | Cathode heater failure due to thermal cycling | Cathode heater failure due to thermal cycling |
| 6. | Cathode ignition failure or excessive performance degradation due to orifice plate erosion | Cathode ignition failure or excessive performance degradation due to orifice plate erosion |
| 7. | Screen grid structural failure due to ion erosion | Screen grid structural failure due to ion erosion |
| 8. | | Arcing through the low-voltage propellant isolator |
| 9. | | Neutralizer clogging at low power |
| 10. | | Cathode ignition failure due to heater erosion |
| 11. | | Excessive performance degradation or cathode ignition failure due to insert depletion |

Table 3. Constant Input Values for the WGW Electron-backstreaming Model.

| | | |
|----------------|----------|--|
| $d_{ai} =$ | 1.143 | Accel. hole diameter BOL (mm) |
| $d_s =$ | 1.905 | Screen hole diameter (mm) |
| $e =$ | 1.60E-19 | Electron charge (coul) |
| $J_e/J_b =$ | 0.1 | Electron-to-ion current ratio that defines EBS |
| $m_e =$ | 9.11E-31 | Electron mass (kg) |
| $m_i =$ | 2.18E-25 | Ion Mass (kg) |
| $V_{bp} =$ | 15 | Beam plasma potential (V) |
| $t_a =$ | 0.508 | Accel. grid thickness (mm) |
| $T_e =$ | 1.80 | Electron temperature in the beam plasma (eV) |
| $t_s =$ | 0.381 | Screen grid thickness (mm) |
| $\epsilon_o =$ | 8.85E-12 | Permittivity of free space (farad/meter) |
| $\rho =$ | 10.22 | Density of molybdenum (mg/mm ³) |

Table 4. Throttle-Level Dependent Input Values for the EBS Model Comparison with the ELT.

| Throttle Level (TH) | Accel. Hole Wall Erosion Rate | Beam Current | Centerline Beamlet Current, J_b | Centerline Beamlet Diameter | V_{dp} | Hot Grid Gap | Effective Acceleration Length, l_e |
|---------------------|-------------------------------|--------------|-----------------------------------|-----------------------------|----------|--------------|--------------------------------------|
| | (mg/khr) | (A) | (mA) | (mm) | (V) | (mm) | (mm) |
| 0 | 0.017 | 0.510 | 0.105 | 0.850 | 650 | 0.460 | 1.271 |
| 1 | 0.018 | 0.530 | 0.108 | 0.762 | 850 | 0.456 | 1.268 |
| 2 | 0.021 | 0.530 | 0.108 | 0.689 | 1000 | 0.456 | 1.268 |
| 3 | 0.026 | 0.610 | 0.122 | 0.679 | 1100 | 0.438 | 1.256 |
| 4 | 0.032 | 0.710 | 0.138 | 0.712 | 1100 | 0.417 | 1.242 |
| 5 | 0.040 | 0.810 | 0.154 | 0.741 | 1100 | 0.395 | 1.228 |
| 6 | 0.049 | 0.910 | 0.169 | 0.767 | 1100 | 0.373 | 1.215 |
| 7 | 0.059 | 1.000 | 0.182 | 0.787 | 1100 | 0.353 | 1.203 |
| 8 | 0.070 | 1.100 | 0.196 | 0.806 | 1100 | 0.332 | 1.190 |
| 9 | 0.081 | 1.200 | 0.209 | 0.822 | 1100 | 0.310 | 1.177 |
| 10 | 0.093 | 1.300 | 0.222 | 0.837 | 1100 | 0.308 | 1.176 |
| 11 | 0.104 | 1.400 | 0.233 | 0.850 | 1100 | 0.306 | 1.175 |
| 12 | 0.116 | 1.490 | 0.244 | 0.862 | 1100 | 0.305 | 1.174 |
| 13 | 0.127 | 1.580 | 0.253 | 0.872 | 1100 | 0.303 | 1.173 |
| 14 | 0.137 | 1.670 | 0.262 | 0.882 | 1100 | 0.302 | 1.172 |
| 15 | 0.146 | 1.760 | 0.270 | 0.891 | 1100 | 0.300 | 1.171 |

Table 5. Throttle-Level Dependent Input Values for the Dawn Thrusters.

| Throttle Level (TH) | Accel. Hole Wall Erosion Rate | Beam Current | Centerline Beamlet Current, J_b | Centerline Beamlet Diameter | V_{dp} | Hot Grid Gap | Effective Acceleration Length, l_e |
|---------------------|-------------------------------|--------------|-----------------------------------|-----------------------------|----------|--------------|--------------------------------------|
| | (mg/khr) | (A) | (mA) | (mm) | (V) | (mm) | (mm) |
| 0 | 0.017 | 0.510 | 0.120 | 0.893 | 650 | 0.460 | 1.271 |
| 1 | 0.018 | 0.530 | 0.125 | 0.801 | 850 | 0.456 | 1.268 |
| 2 | 0.021 | 0.530 | 0.125 | 0.722 | 1000 | 0.456 | 1.268 |
| 3 | 0.026 | 0.610 | 0.144 | 0.716 | 1100 | 0.438 | 1.256 |
| 4 | 0.032 | 0.710 | 0.167 | 0.757 | 1100 | 0.417 | 1.242 |
| 5 | 0.040 | 0.810 | 0.188 | 0.791 | 1100 | 0.395 | 1.228 |
| 6 | 0.049 | 0.910 | 0.206 | 0.819 | 1100 | 0.373 | 1.215 |
| 7 | 0.059 | 1.000 | 0.221 | 0.839 | 1100 | 0.353 | 1.203 |
| 8 | 0.070 | 1.100 | 0.236 | 0.856 | 1100 | 0.332 | 1.190 |
| 9 | 0.081 | 1.200 | 0.250 | 0.869 | 1100 | 0.310 | 1.177 |
| 10 | 0.093 | 1.300 | 0.261 | 0.882 | 1100 | 0.308 | 1.176 |
| 11 | 0.104 | 1.400 | 0.270 | 0.892 | 1100 | 0.306 | 1.175 |
| 12 | 0.116 | 1.490 | 0.277 | 0.899 | 1100 | 0.305 | 1.174 |
| 13 | 0.127 | 1.580 | 0.282 | 0.904 | 1100 | 0.303 | 1.173 |
| 14 | 0.137 | 1.670 | 0.285 | 0.908 | 1100 | 0.302 | 1.172 |
| 15 | 0.146 | 1.760 | 0.287 | 0.910 | 1100 | 0.300 | 1.171 |

Table 6. Erosion Curve Fit Coefficients

| Parameter | Hole Wall Erosion BOL and EOL | Pits & Grooves Erosion BOL | Pits & Grooves Erosion EOL |
|--------------------|-------------------------------|----------------------------|----------------------------|
| a_0 | 1.224×10^{-1} | 1.316×10^{-1} | 1.480×10^{-1} |
| a_1 | -2.653×10^{-3} | -8.106×10^{-4} | -2.058×10^{-2} |
| a_2 | 8.438×10^{-3} | 5.590×10^{-3} | 1.600×10^{-2} |
| a_3 | -2.784×10^{-4} | -2.473×10^{-4} | -7.208×10^{-4} |
| \dot{m}_{TH15} | 0.141 mg/khr | N/A | |
| \dot{m}''_{TH15} | N/A | | 0.210 mg/khr |

Table 7. Ranges of Key Input Parameters for the PFA Formulation of the EBS Model.

| Parameter | Range |
|--|--------------------|
| Sputter Erosion Rates | +/- 15% |
| Propellant Flow Rates | +/- 3% |
| Beamlet Current | +/- 10% |
| Beamlet Diameter | +/- 10% |
| Hot Grid Gap | +/- 0.02 mm |
| Minimum hole diameter after cusp removal | +/- 0.01 mm |
| Minimum hole diameter at which chamfering starts | +/- 0.02 mm |
| Width of Pit & Grooves erosion pattern | 450 to 575 microns |
| Beam plasma potential | +/- 5 V |
| Electron Temperature in the beam plasma | +/- 1.0 eV |

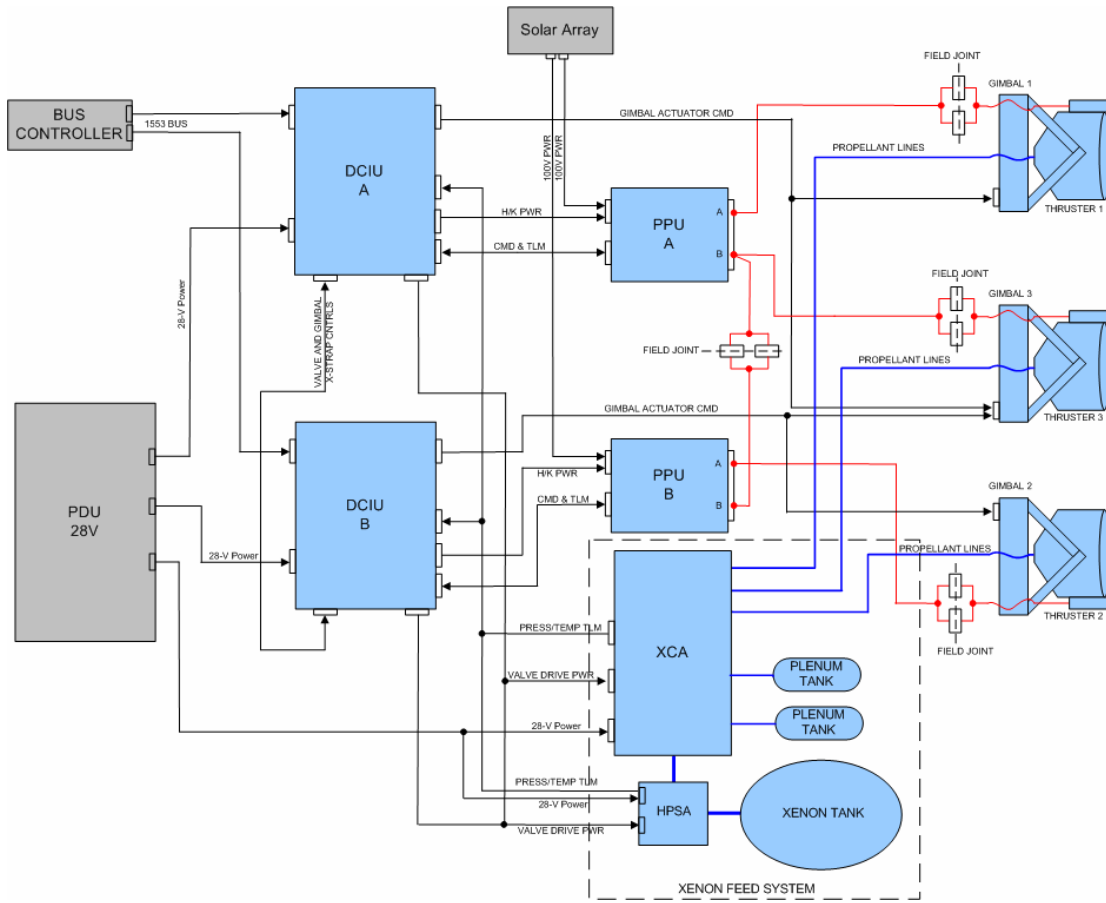


Fig. 1. Simplified IPS block diagram.

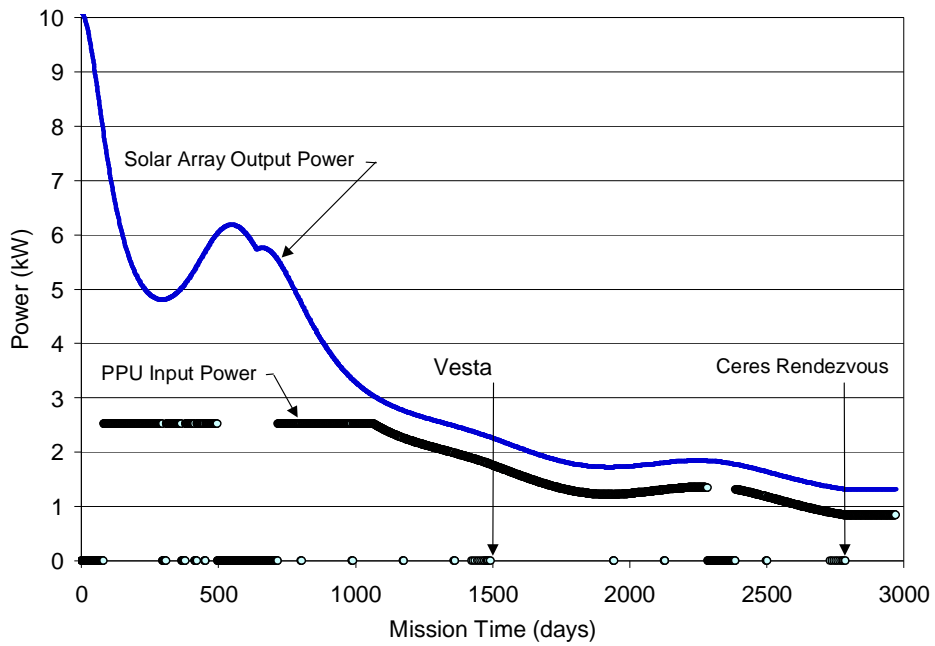


Fig. 2. Solar array output power and PPU input power during the Dawn mission for a representative trajectory.

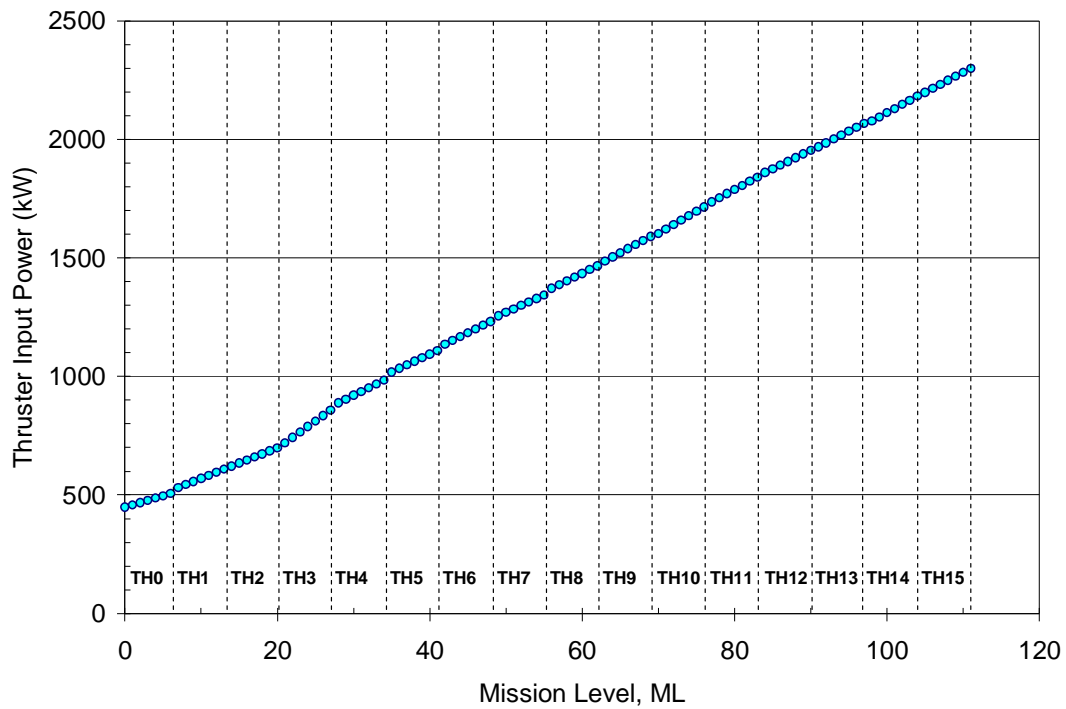


Fig. 3. Illustration of the ion thruster mission levels (ML) and throttle levels (TH).

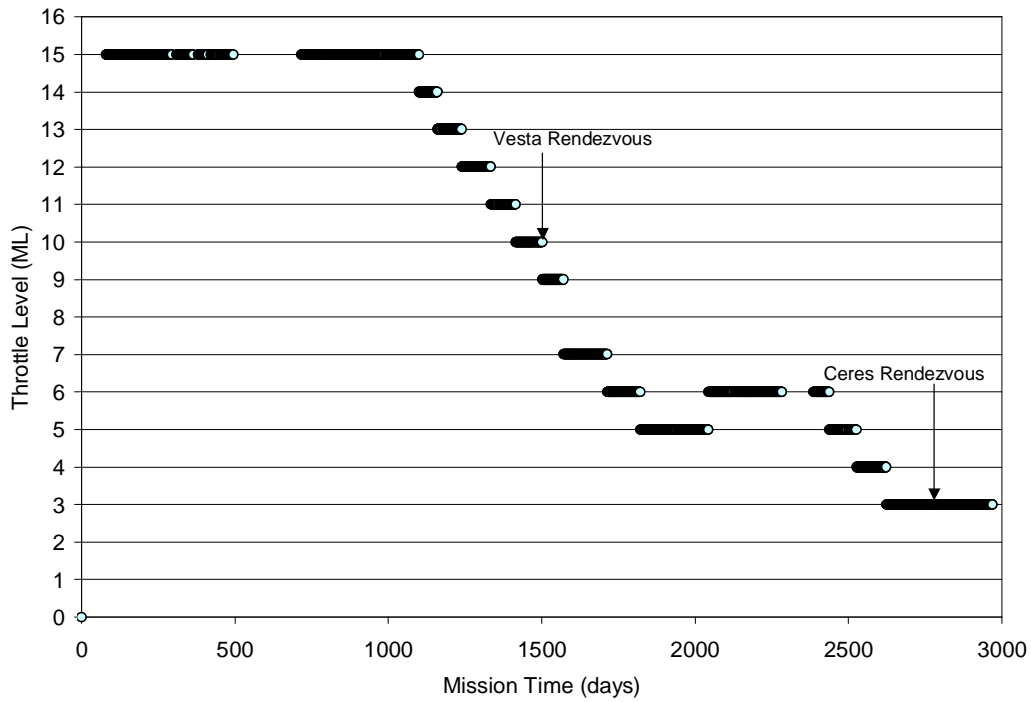


Fig. 4. Variation in throttle level (TH) with mission time.

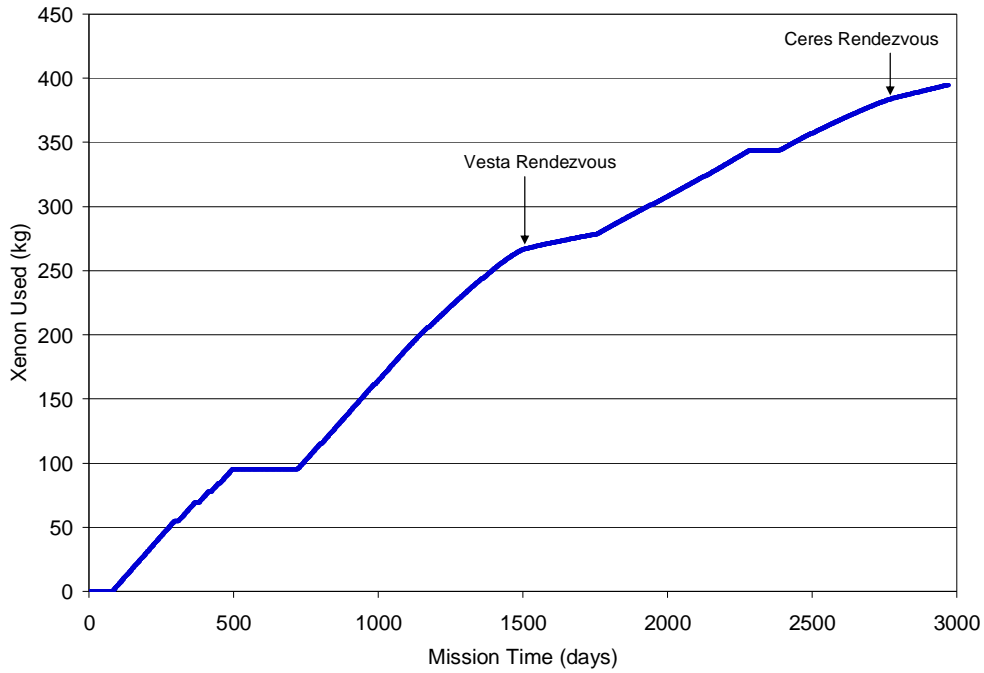


Fig. 5. Xenon process as a function of mission time.

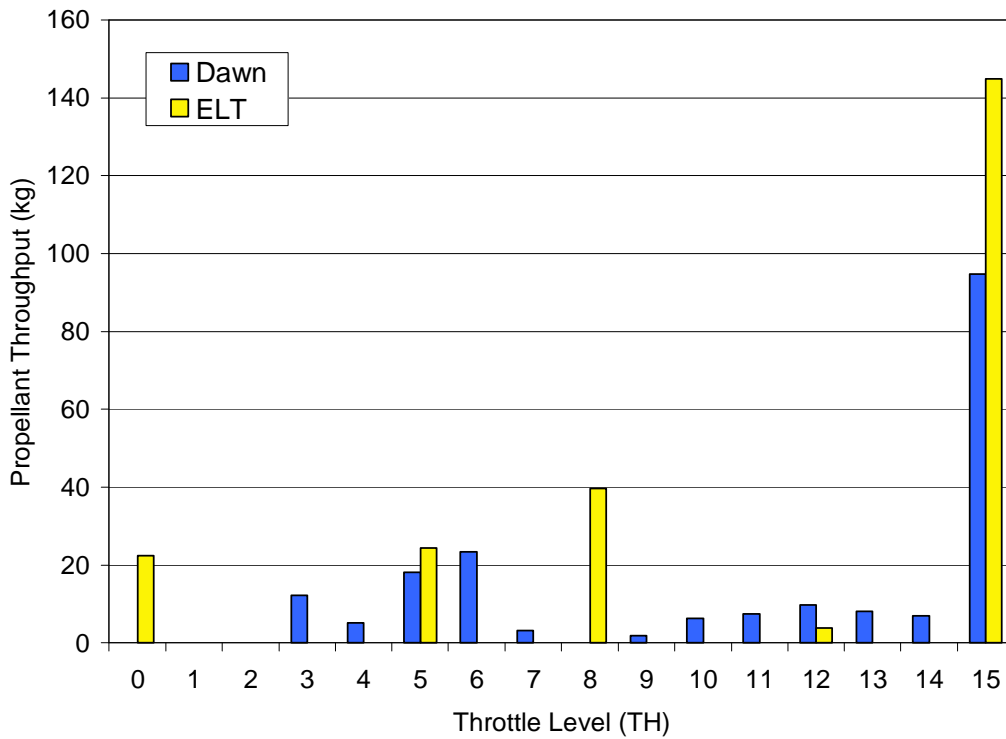


Fig. 6. Comparison of xenon usage per throttle level for the case where only two thrusters are used for the entire Dawn mission and these thrusters share the propellant throughput equally at every throttle level.

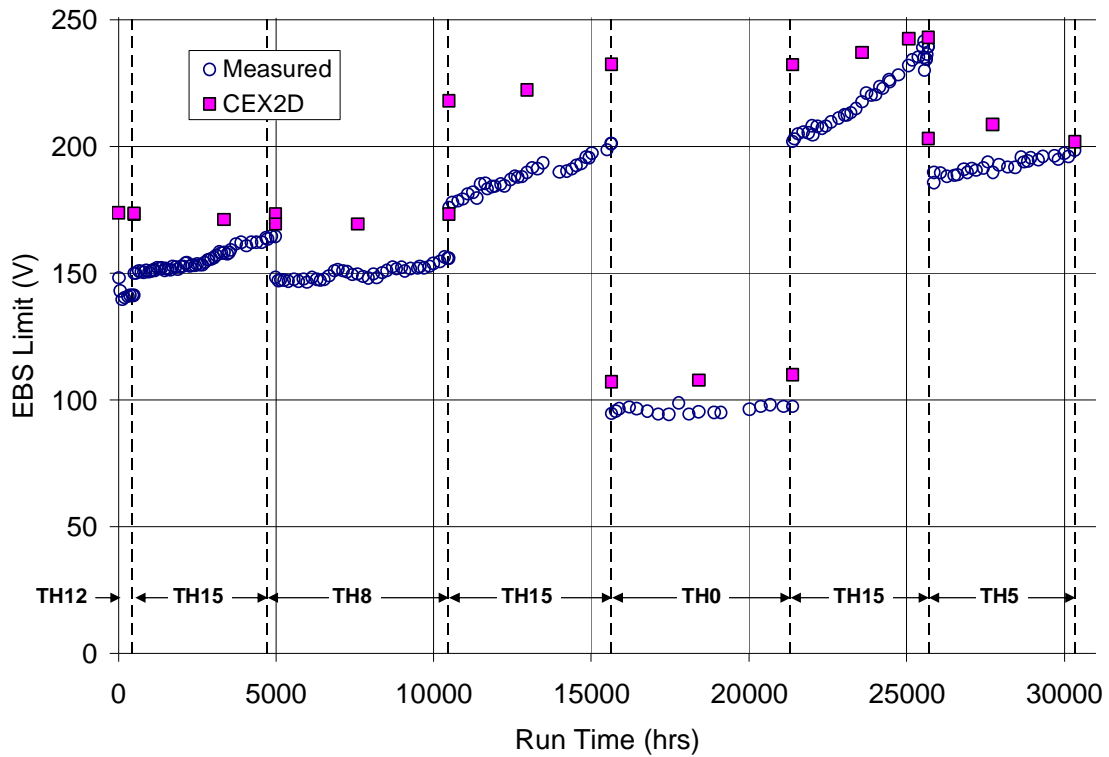


Fig. 7. Variation in the magnitude of the electron-backstreaming voltage measured during the ELT.

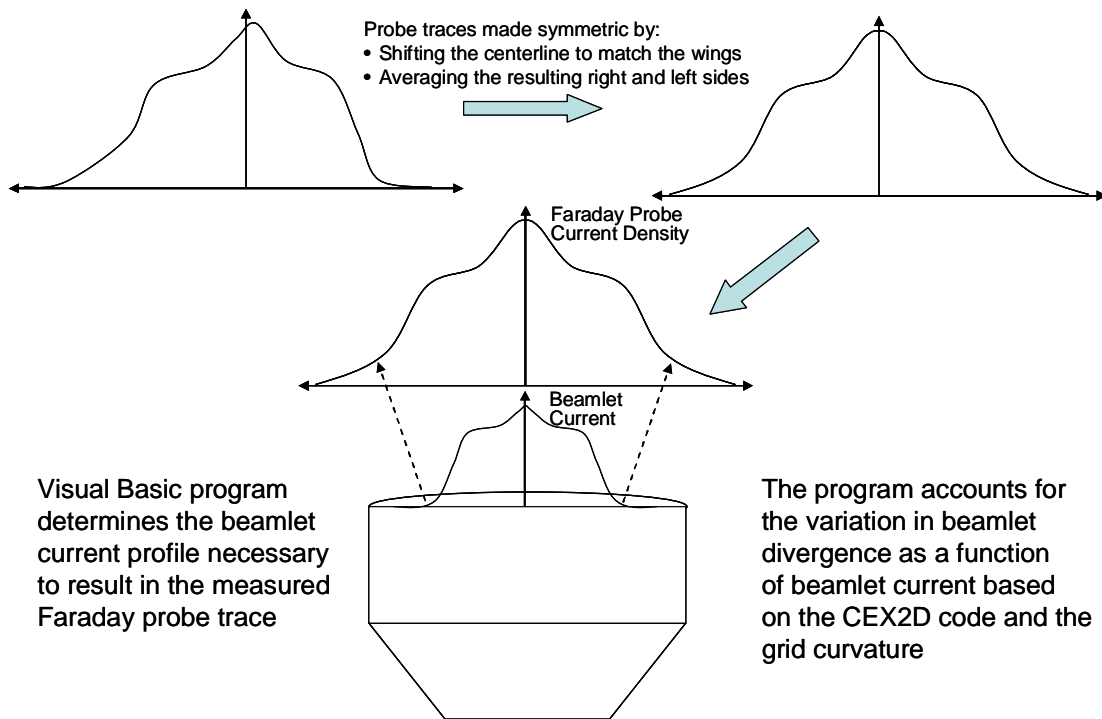


Fig. 8. Procedure used to extract beamlet currents from measured Faraday probe data.

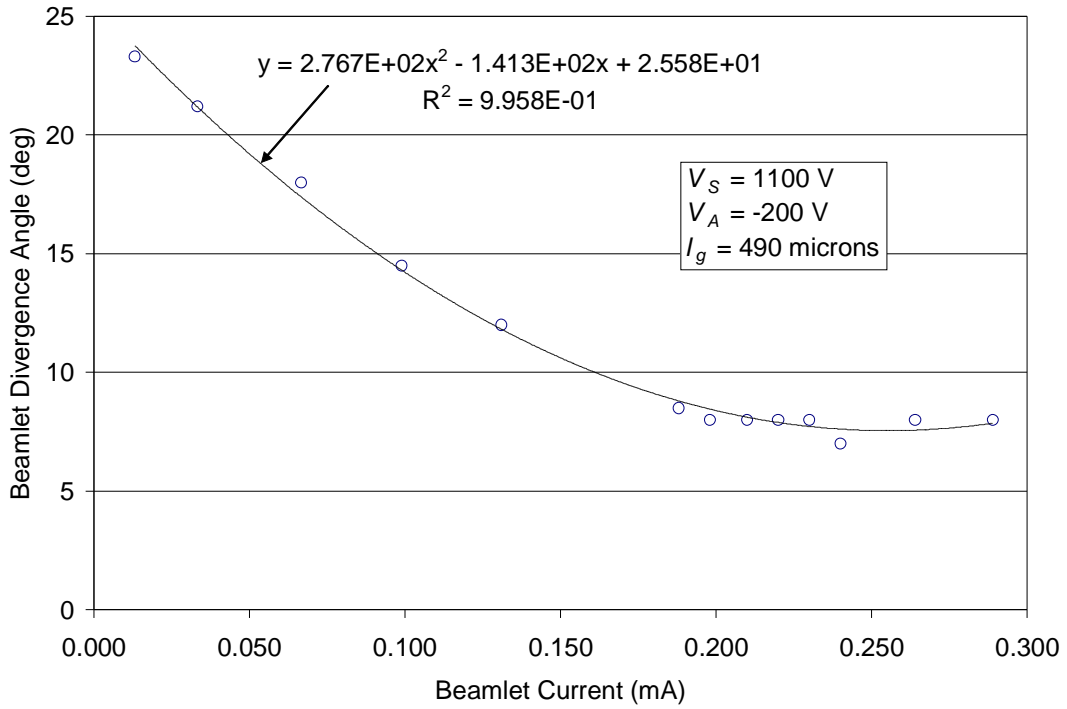


Fig. 9. Beamlet divergence angles as a function of beamlet current from the CEX2D code.

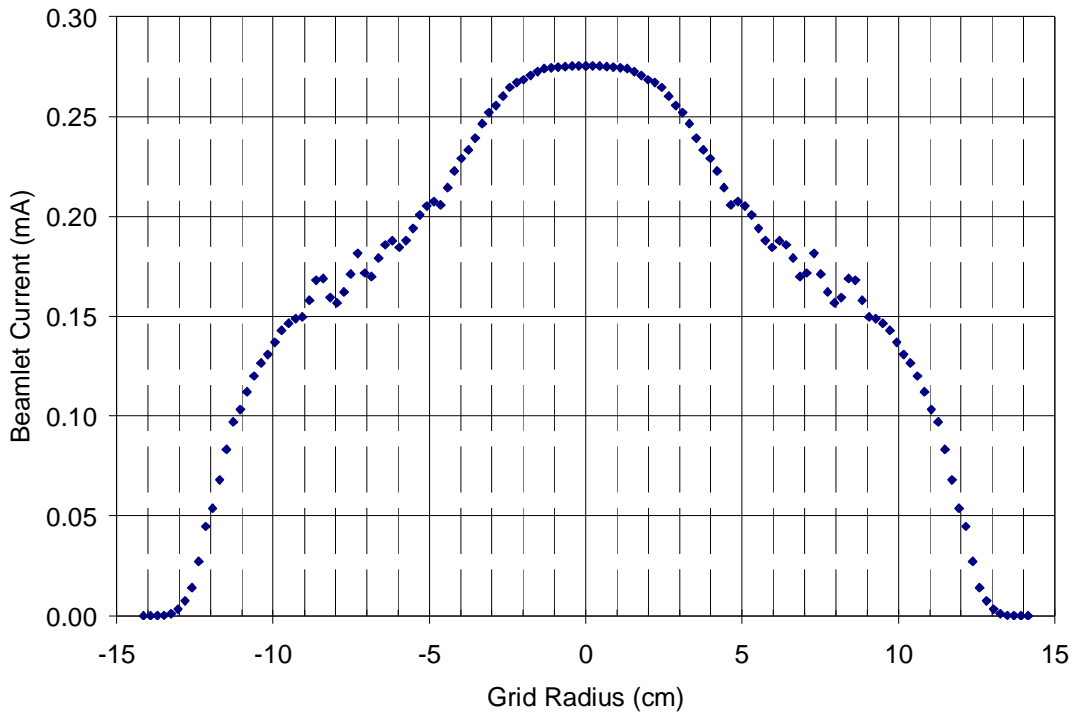


Fig. 10. Calculated beamlet profile for FT003 operating at TH15 unpacked from measured Faraday probe data.

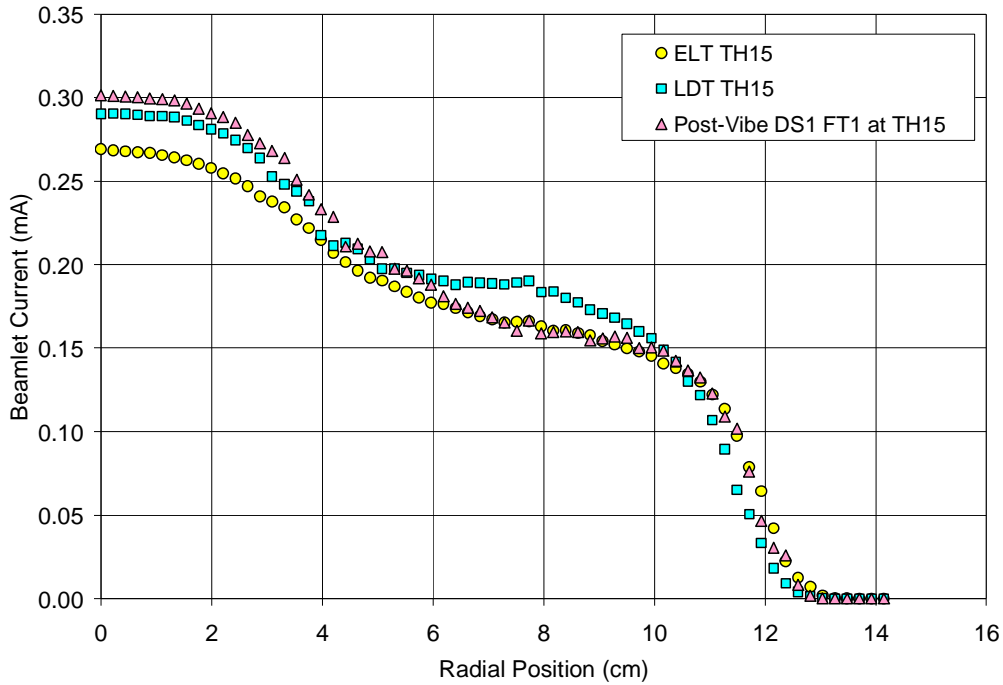


Fig. 11. Comparison of calculated beamlet profiles based on measured Faraday probe traces for the LDT thruster and the two DS1 flight thrusters at TH15.

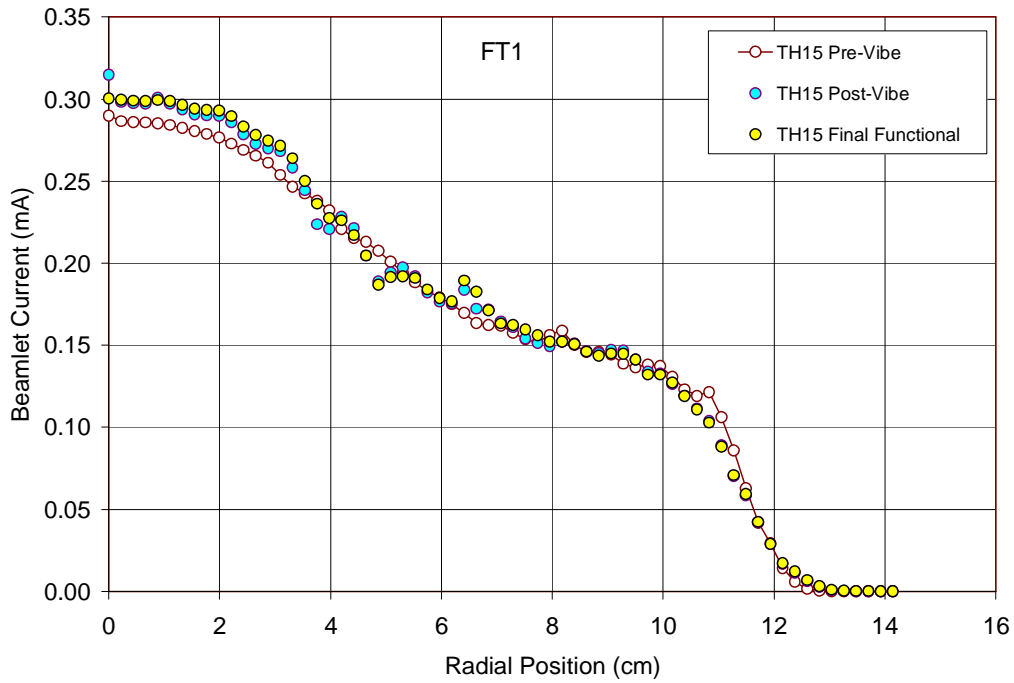


Fig. 12. Beamlet profile for Dawn FT001 at TH15.

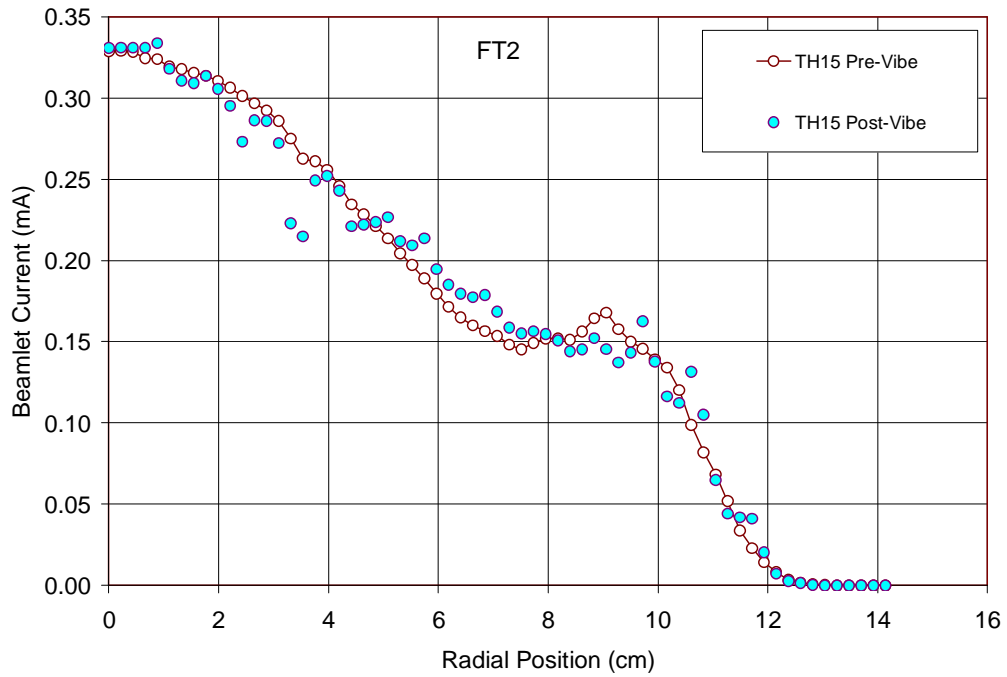


Fig. 13. Beamlet profile for Dawn FT002 at TH15.

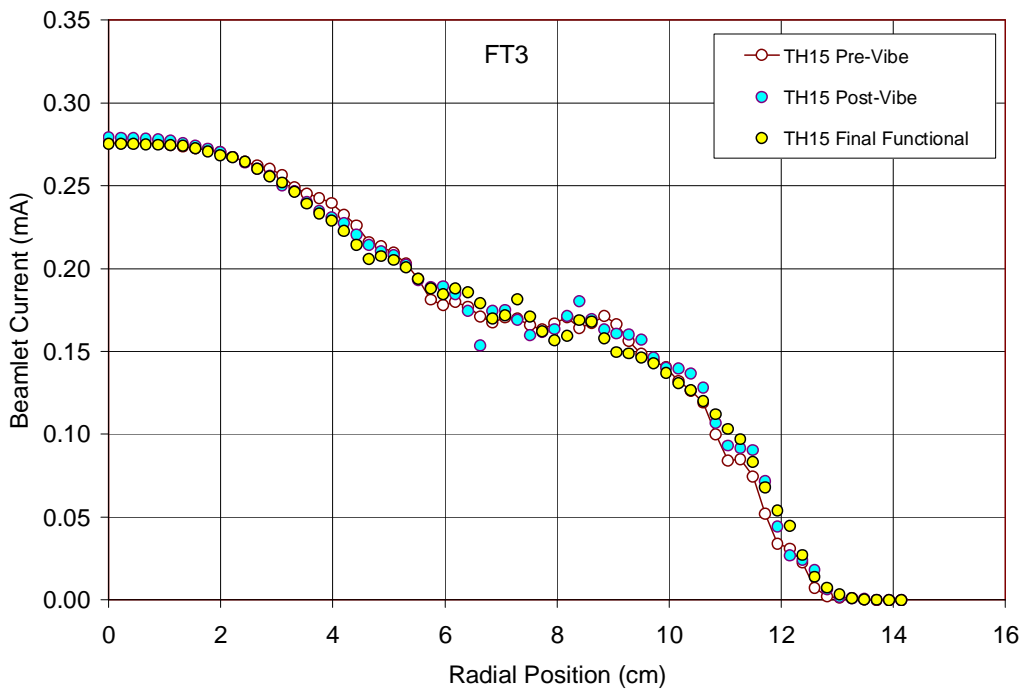


Fig. 14. Beamlet profile for Dawn FT003 at TH15.

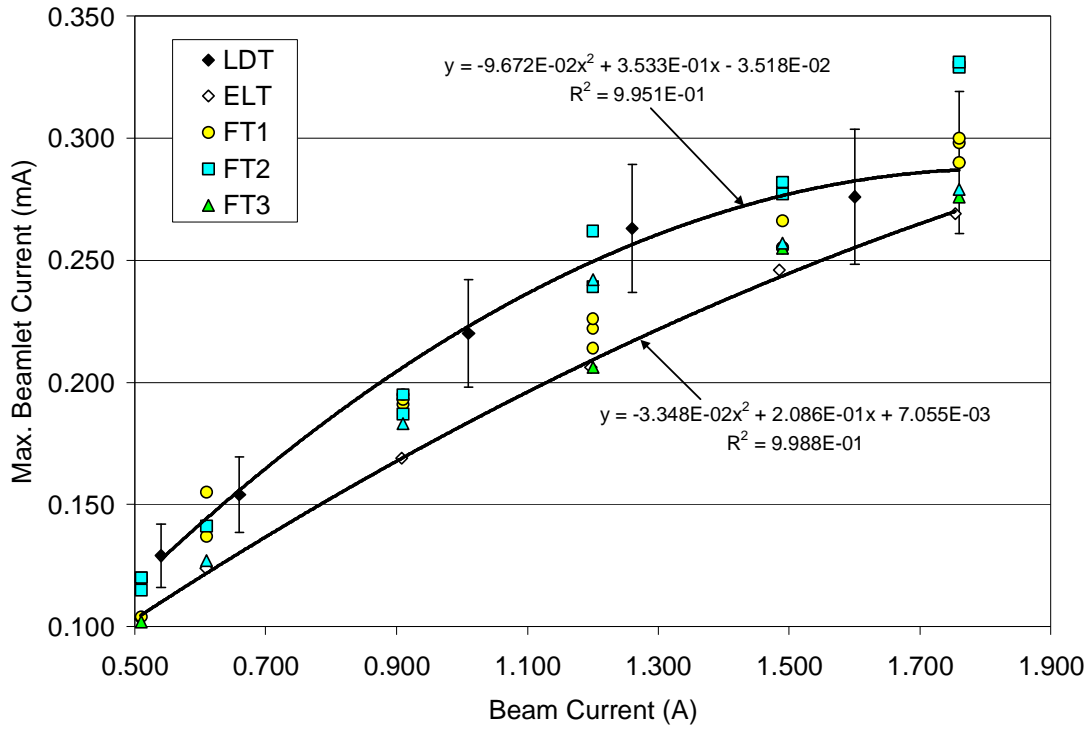


Fig. 15. Peak beamlet currents for the Dawn ion thrusters over the full throttle range.

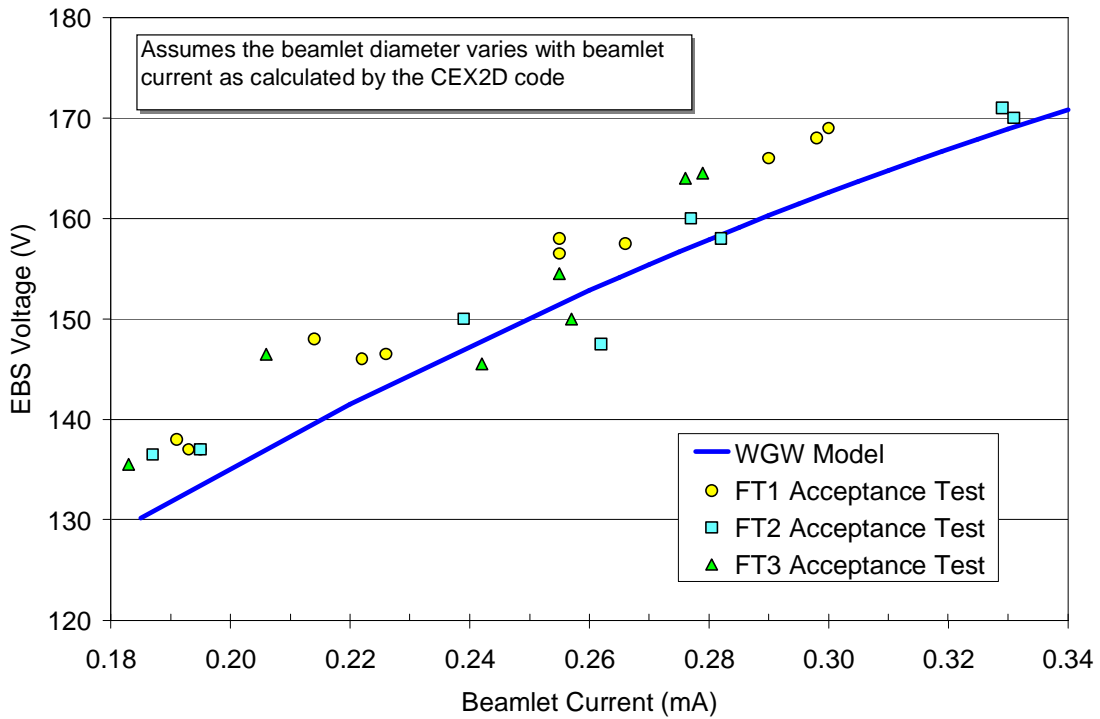


Fig. 16. Measured variation in the EBS voltage with peak beamlet current for beginning of life grid geometry.

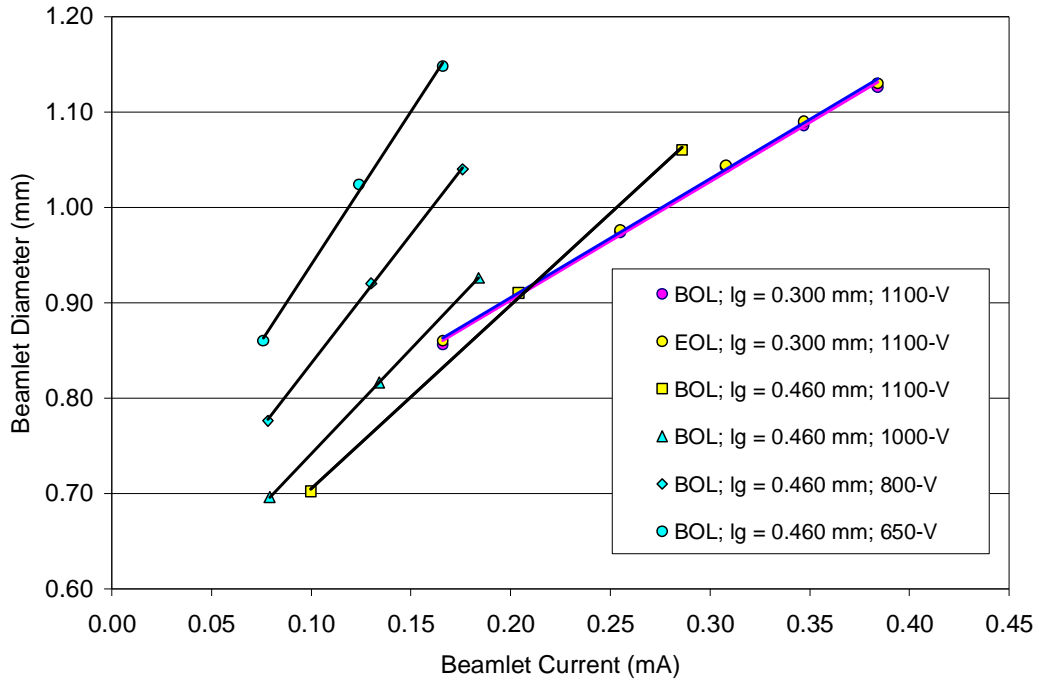


Fig. 17. CEX2D-calculated beamlet diameters as a function of beamlet current, grid gap, and beam voltage. Note the change in slopes for different grid gaps (l_g).

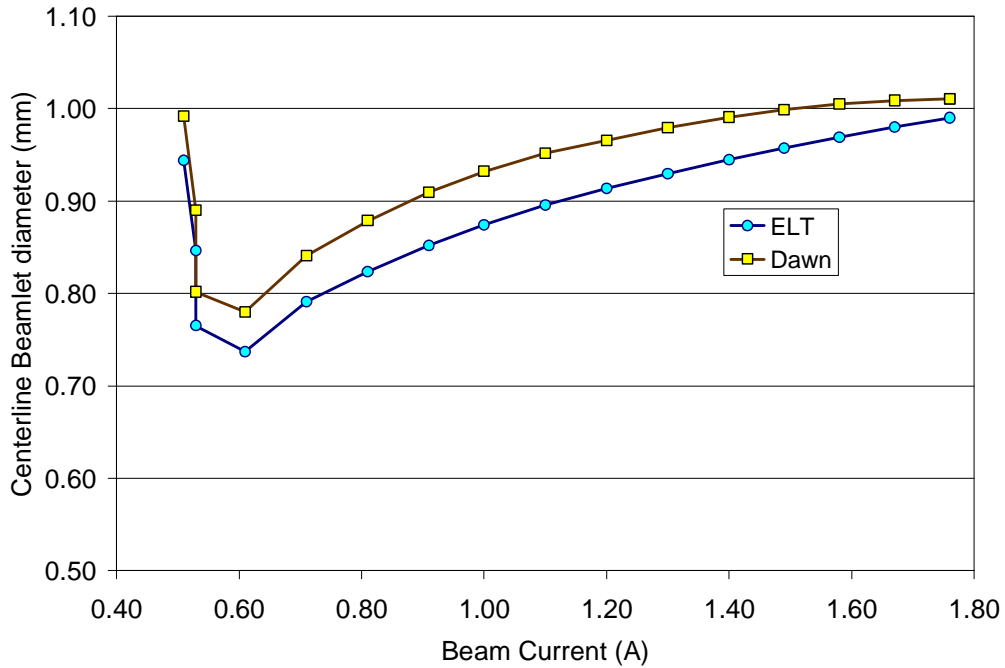


Fig. 18. Centerline beamlet diameters from the CEX2D code multiplied by 0.9.

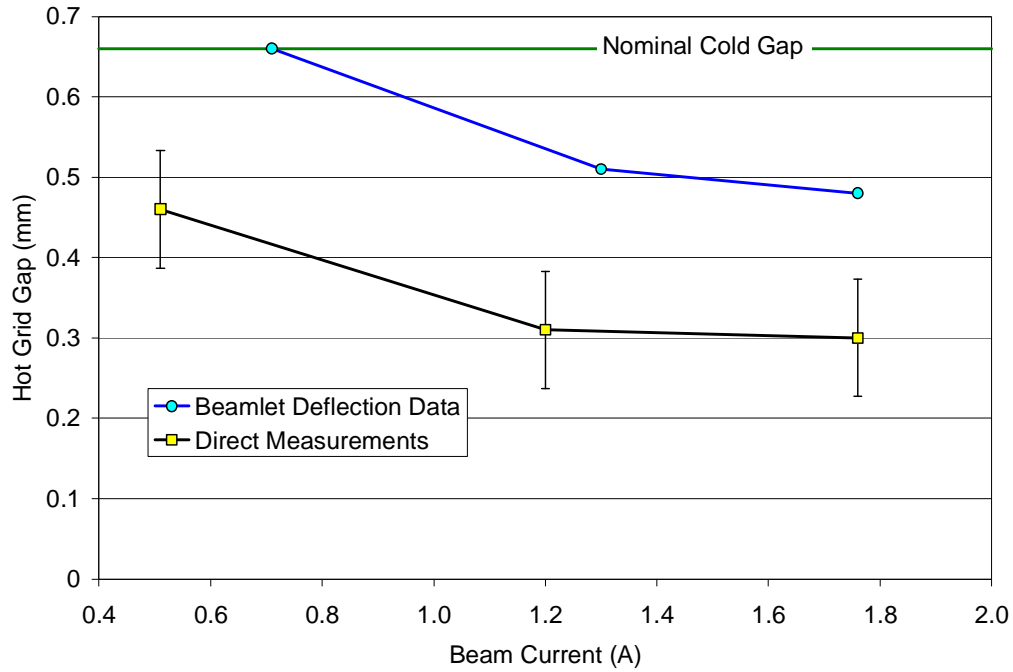


Fig. 19. Comparison of hot-grid gap data showing a large differences between measurement approaches. The direct measurements were used in the EBS analysis.

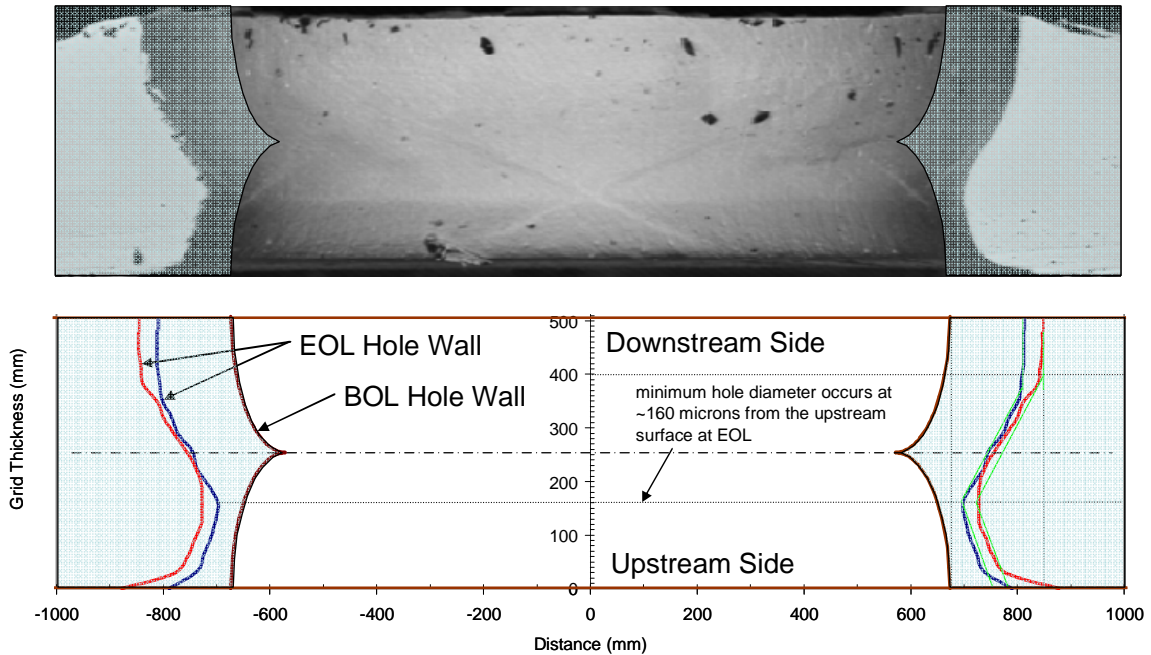


Fig. 20. Accelerator grid hole wall geometry at beginning-of-life (BOL) and end-of-life (EOL) from the ELT.

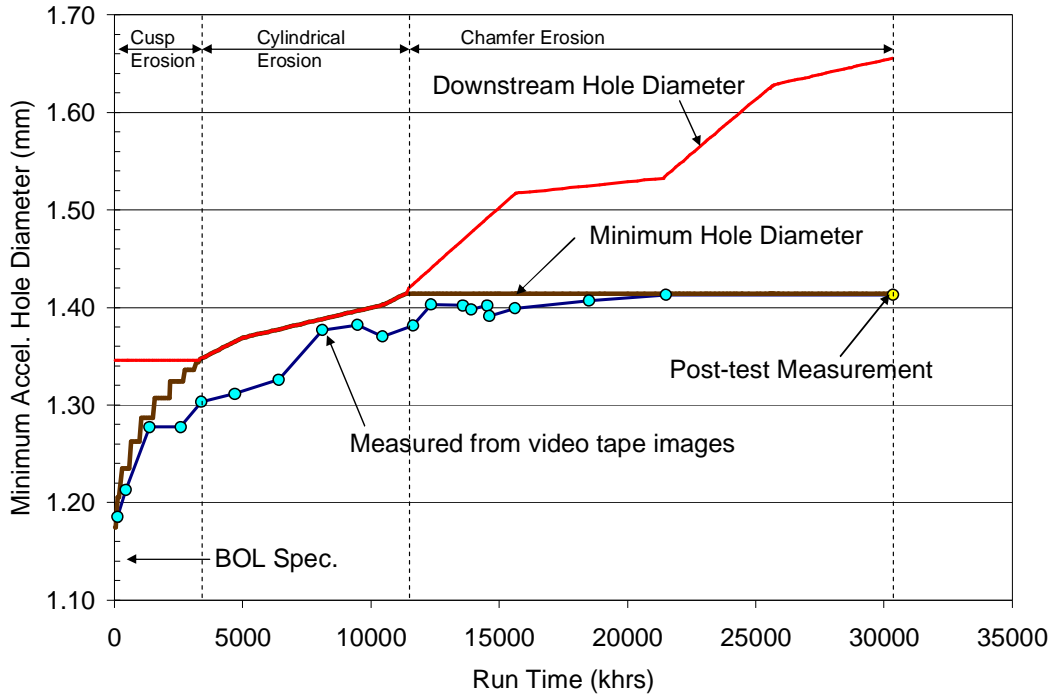


Fig. 21. Measured minimum accelerator hole diameters on the thruster centerline from the ELT are compared to the semi-empirical model of the grid erosion.

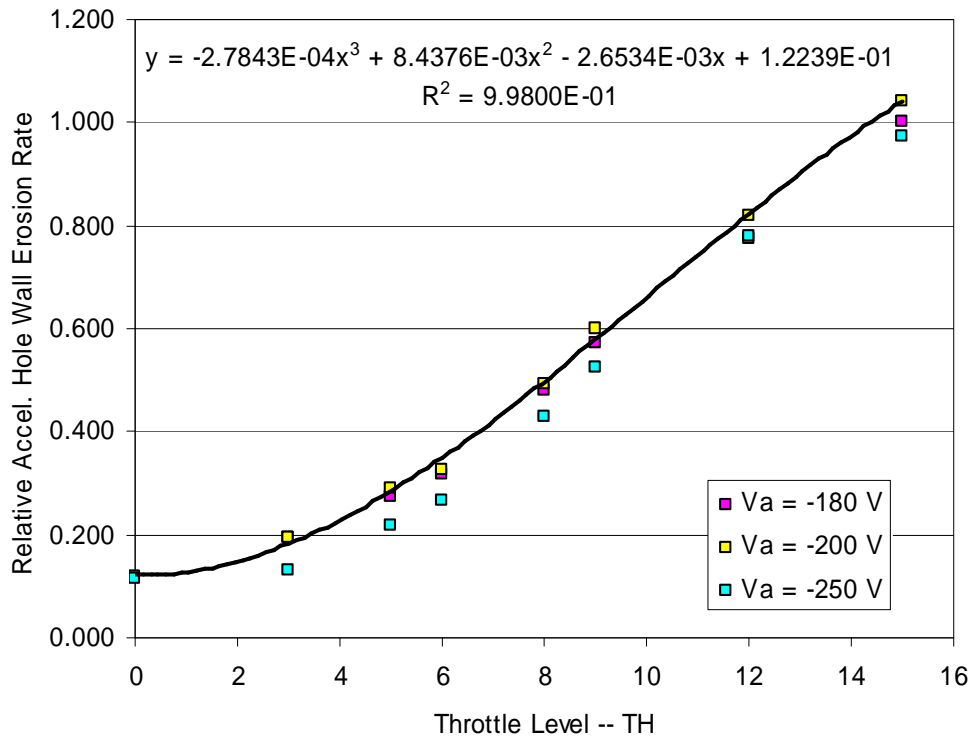


Fig. 22. Accelerator hole wall erosion rates, based on the CEX2D code, normalized by the calculated rate at TH15 with $V_A = -180$ V.

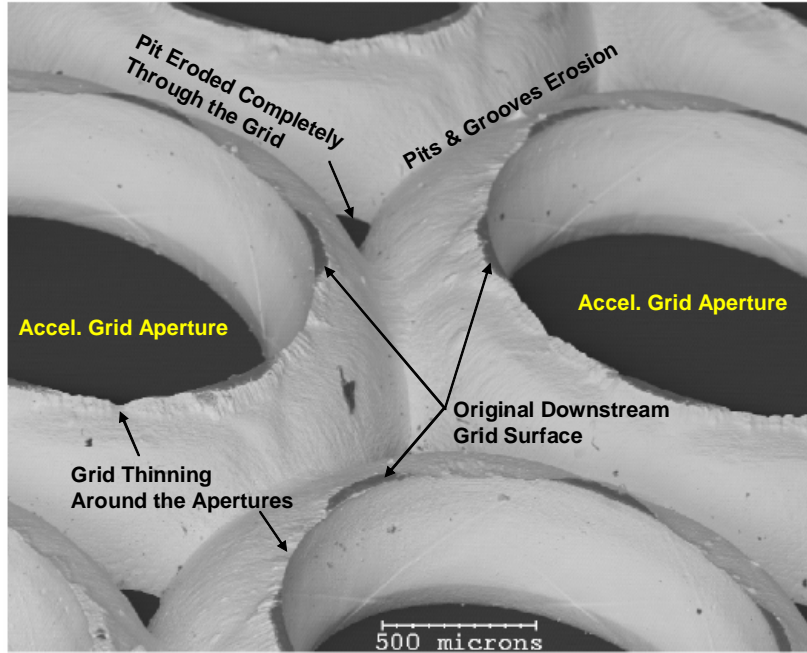


Fig. 23. SEM photograph of the downstream surface of the ELT accelerator grid after the test showing grid thinning around the accelerator apertures due to the intersection of the hole-wall erosion with the pits & grooves erosion.

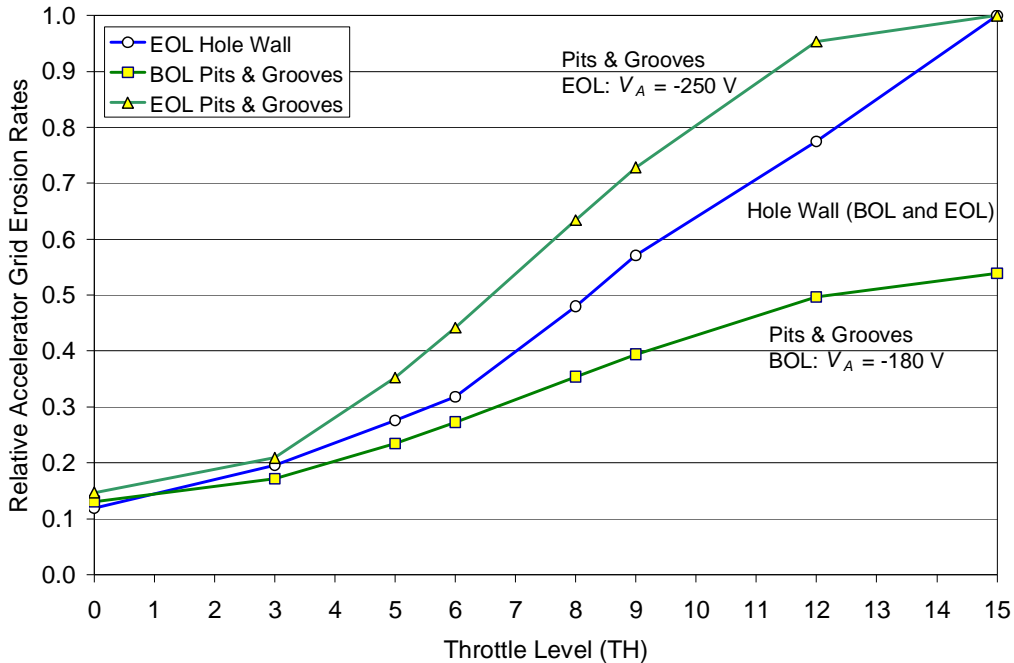


Fig. 24. Normalized variation in erosion rates determined from the CEX2D code.

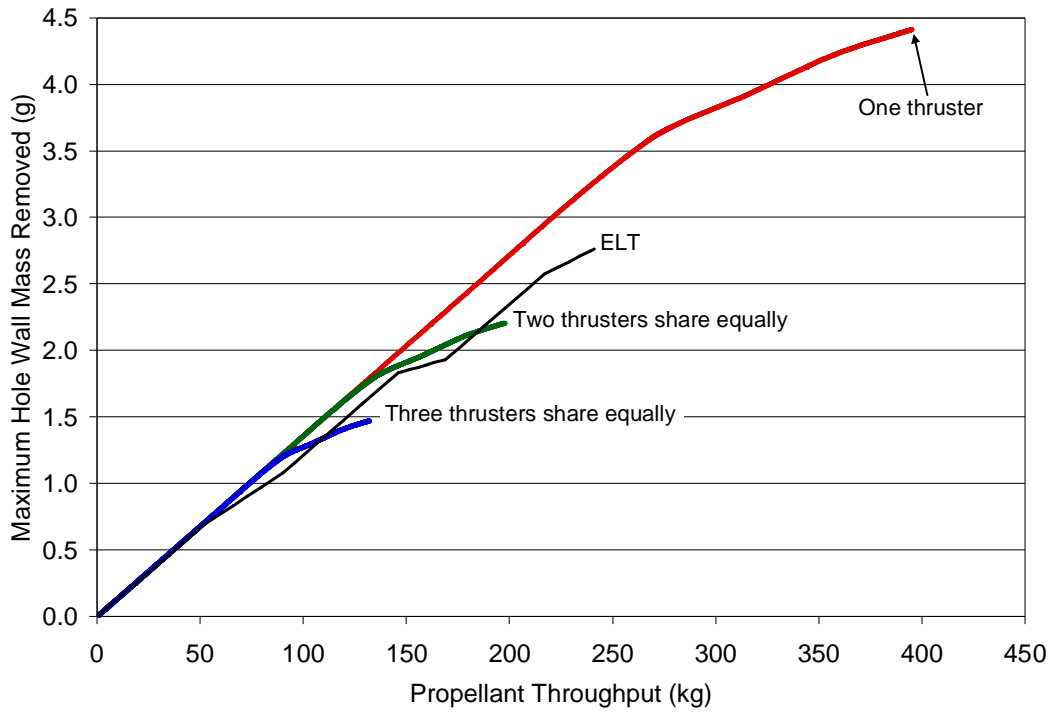


Fig. 25. Maximum calculated accelerator grid hole wall erosion for three Dawn Mission scenarios and the ELT.

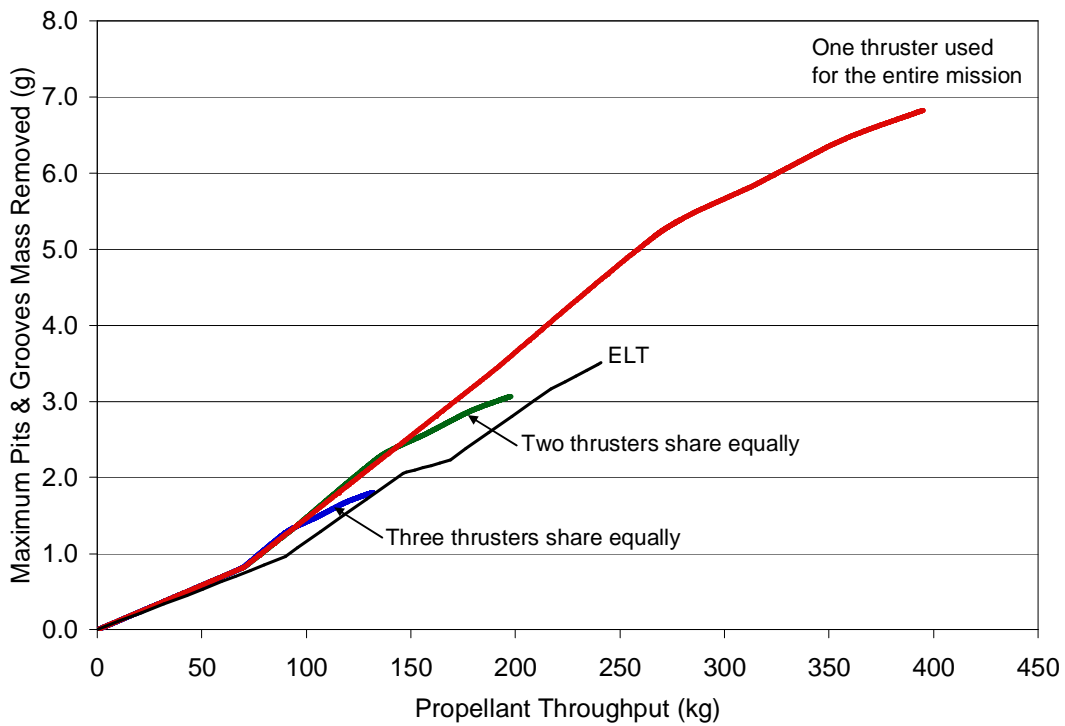


Fig. 26. Maximum calculated pits & grooves erosion for three Dawn Mission scenarios and the ELT.

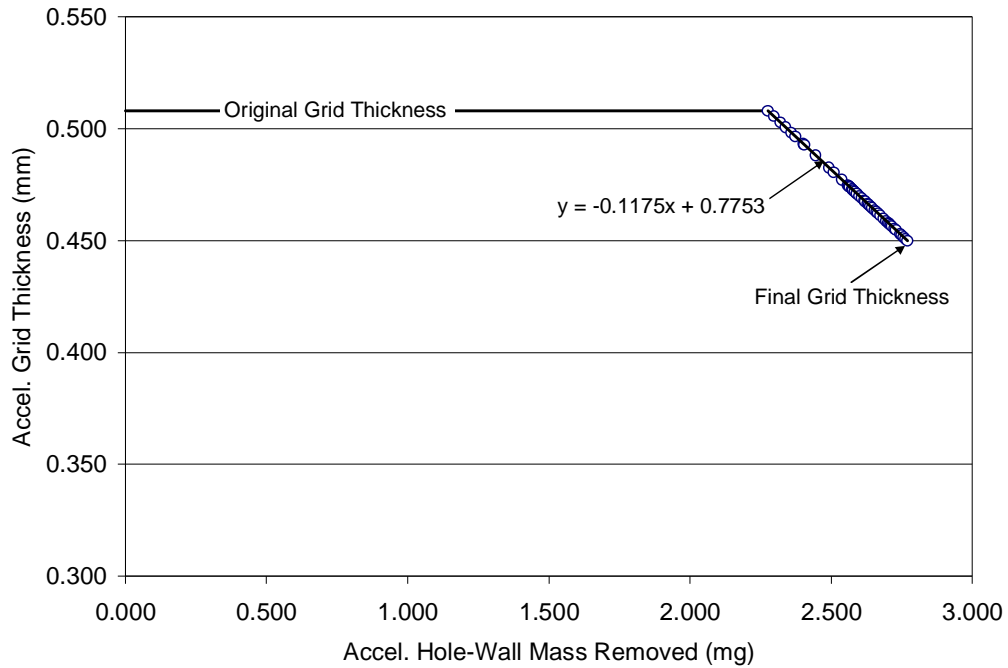


Fig. 27. Assumed variation in accelerator grid thickness with the mass removed from the accelerator grid hole wall.

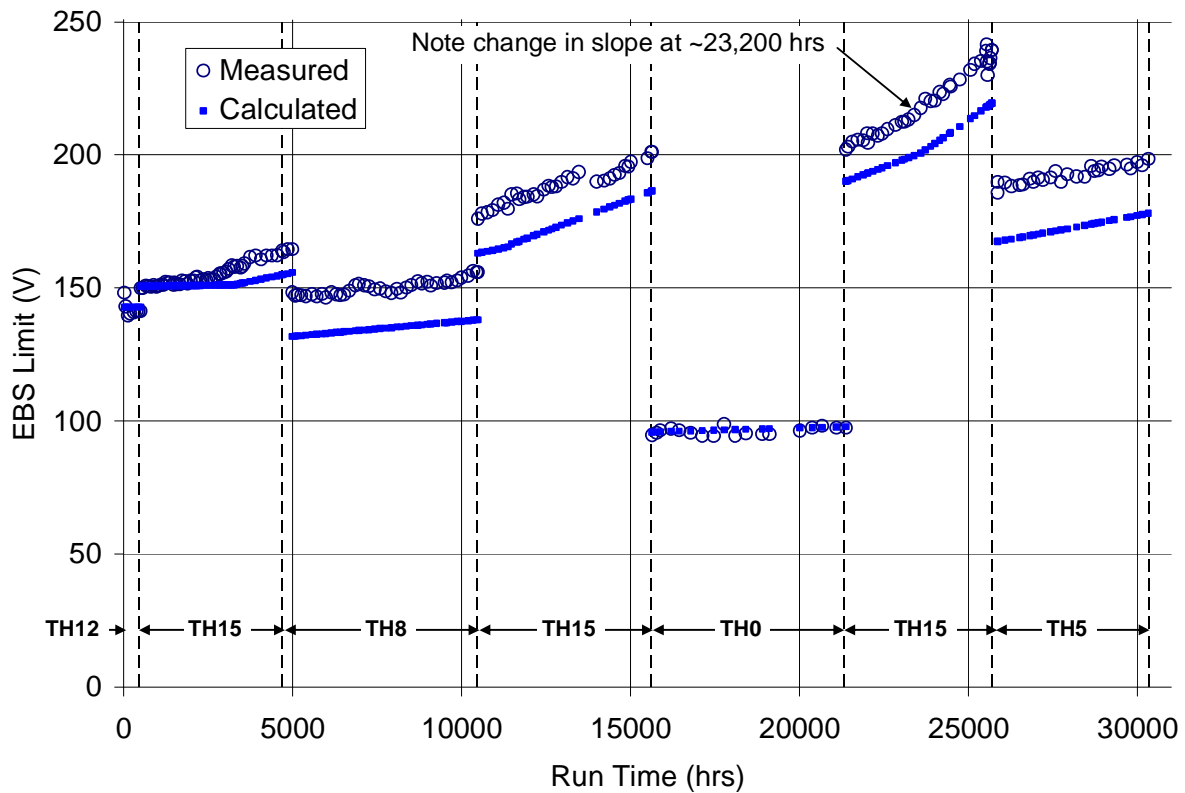


Fig. 28. Comparison of the WGW model for EBS with the ELT data

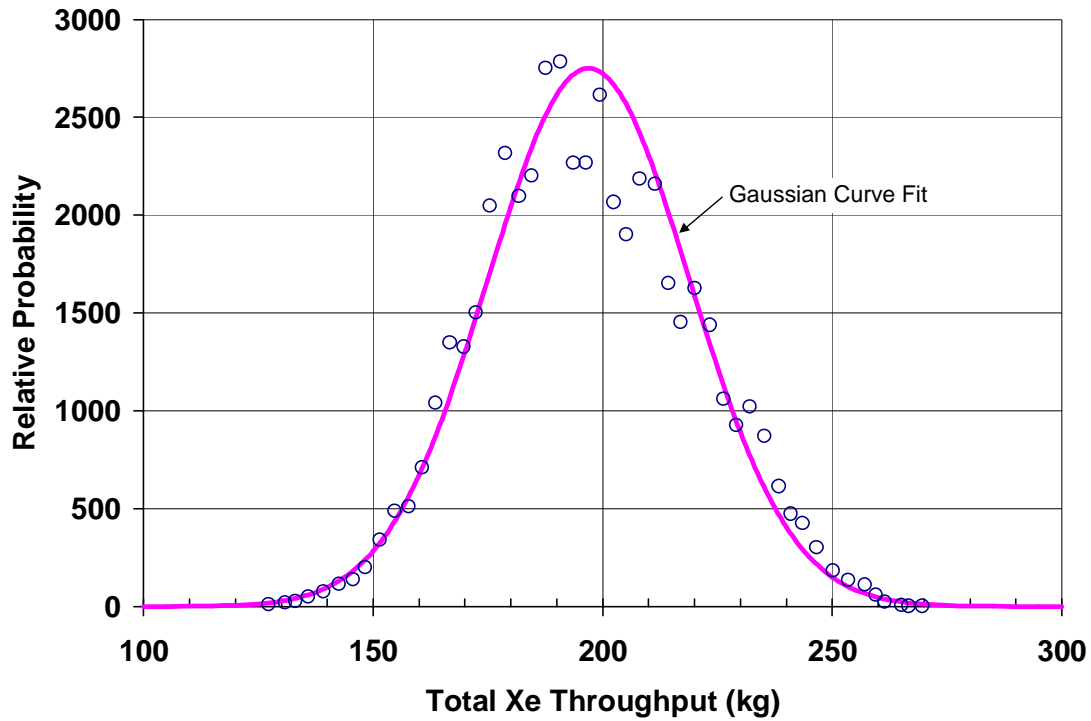


Fig. 29. Calculated failure distribution for the NSTAR ion thruster operating at full power. Gaussian curve fit has a standard deviation of 23 kg.

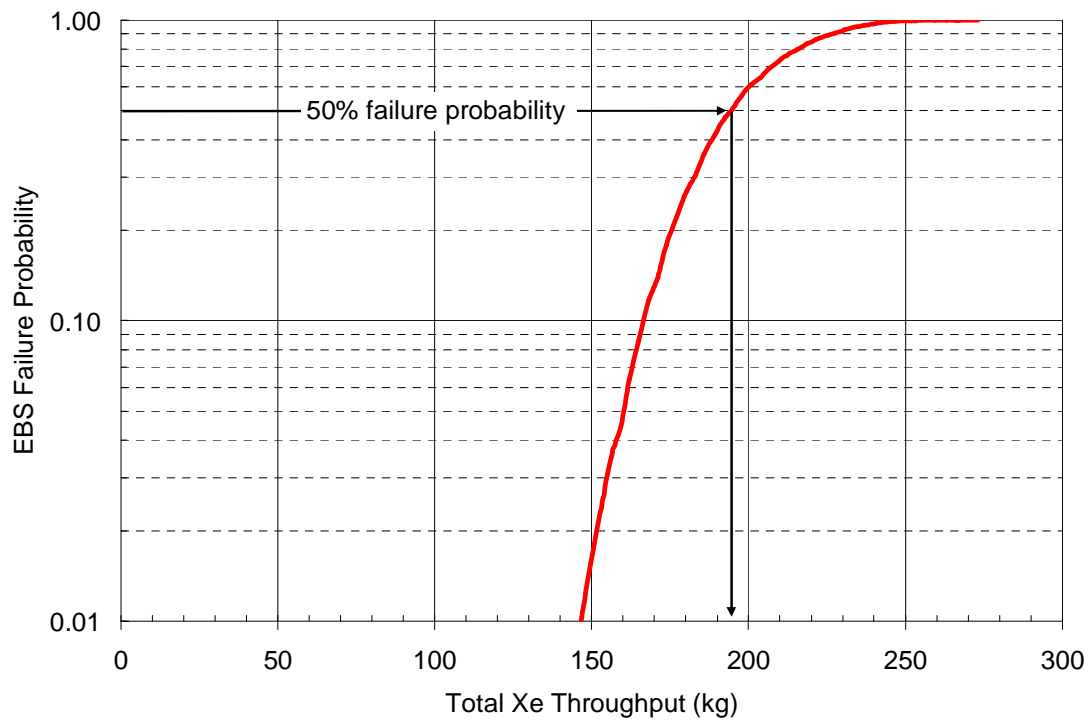


Fig. 30. Probability of grid failure from electron-backstreaming as a function of the propellant throughput at full power (TH15).

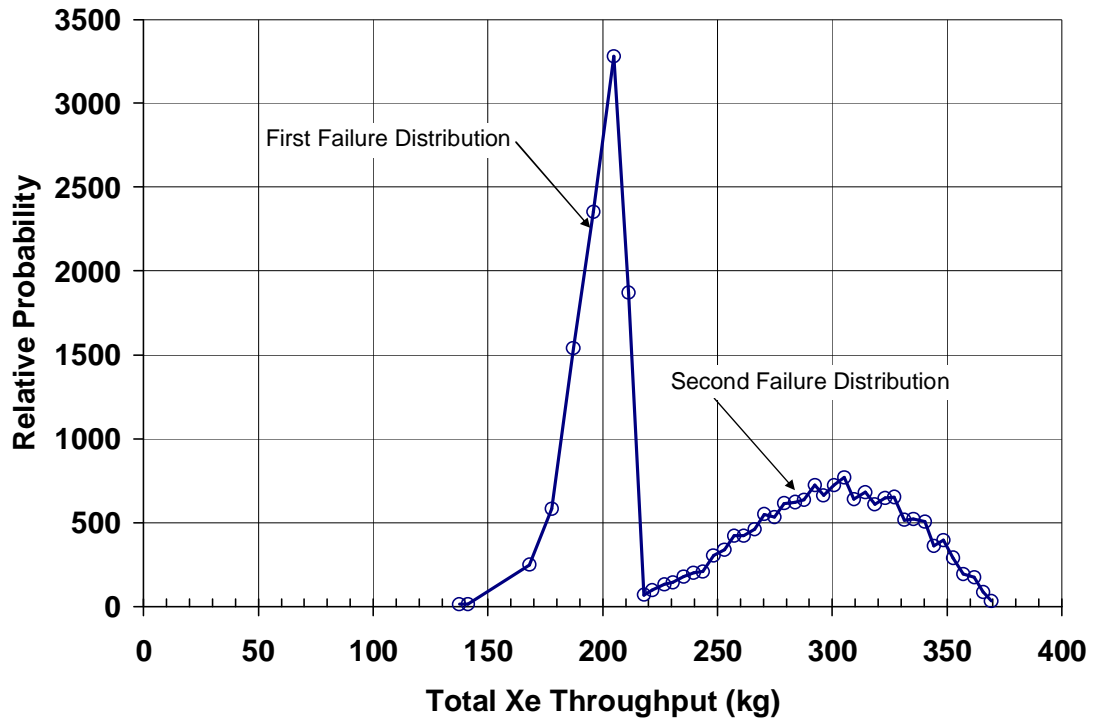


Fig. 31. Calculated failure distribution for the NSTAR ion thruster in the ELT.

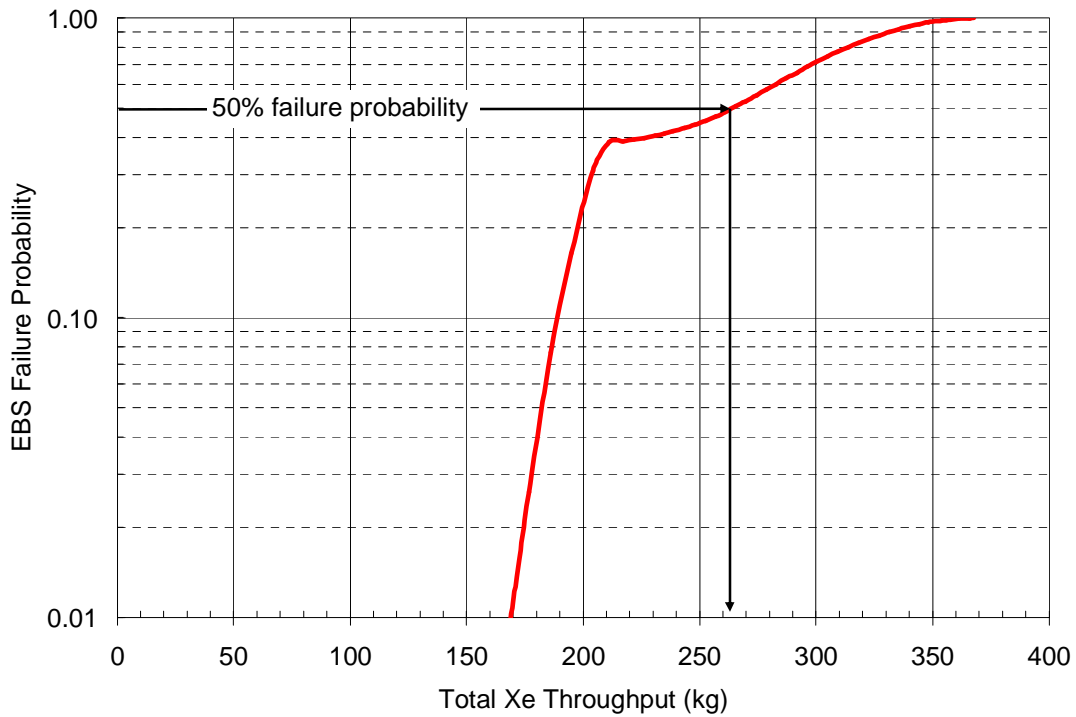


Fig. 32. Calculated failure probability for the NSTAR ion thruster in the ELT.

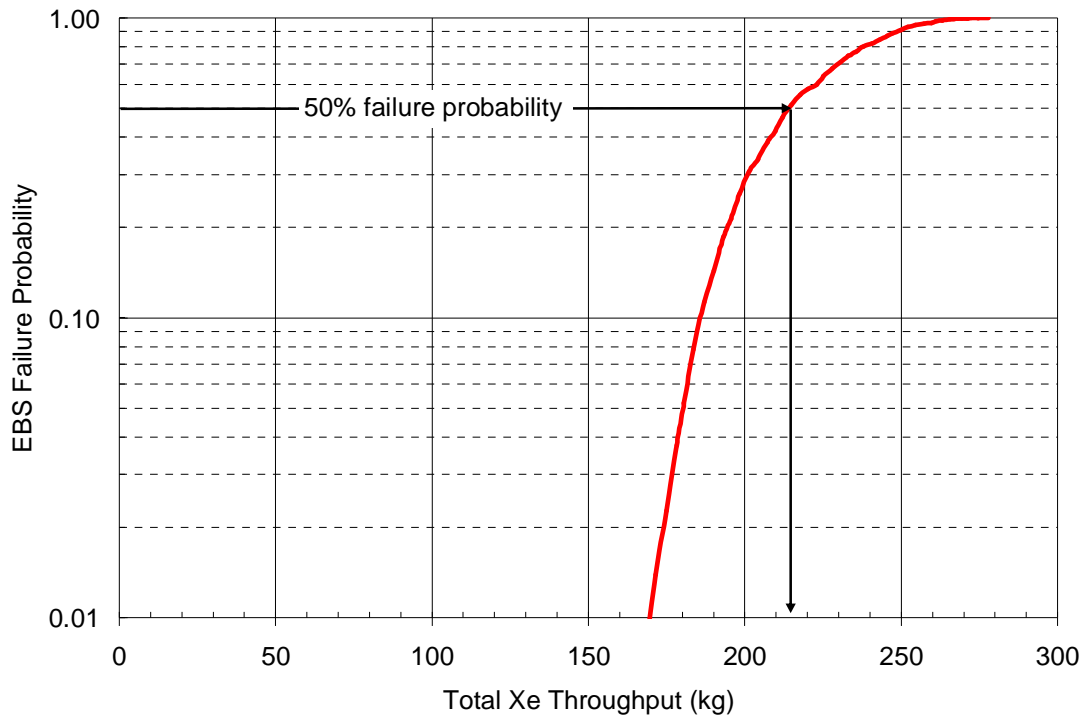


Fig. 33. Calculated failure probability for a single Dawn thruster used for the entire mission. There is a 100% probability that the thruster will fail due to accelerator grid erosion before processing the 395 kg of xenon required to complete the mission.

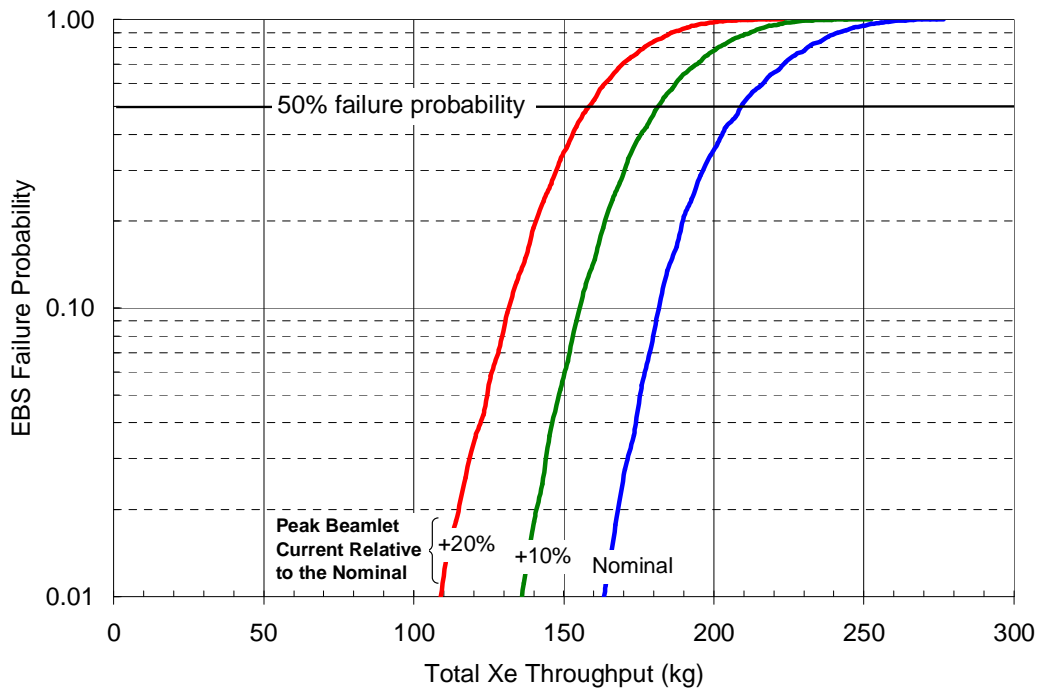


Fig. 34. The effect of peak beamlet current on the calculated failure probability for operation at TH15.

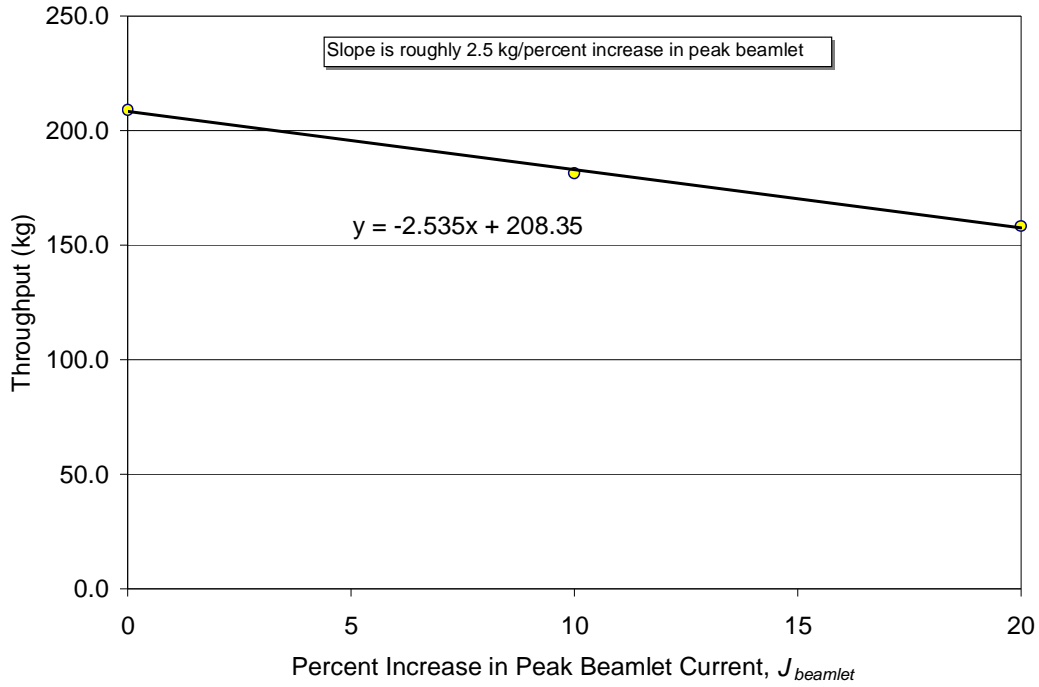


Fig. 35. The propellant throughput capability based on grid life at TH15 is a linear function of the peak beamlet current with a slope of -2.5 kg / percent increase.

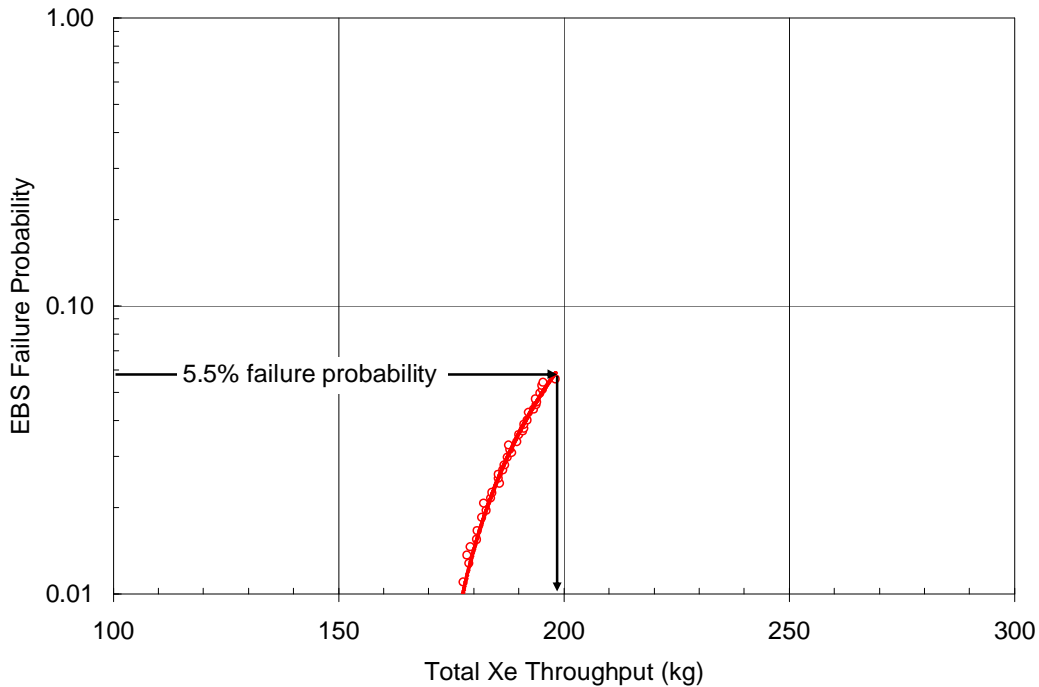


Fig. 36. Calculated failure probability for FT2 based on accelerator grid erosion assuming that FT2 and one other thruster are used for the entire mission and that these two thrusters share the propellant throughput equally at every throttle level. There is a 1% failure probability at a throughput of 178 kg.

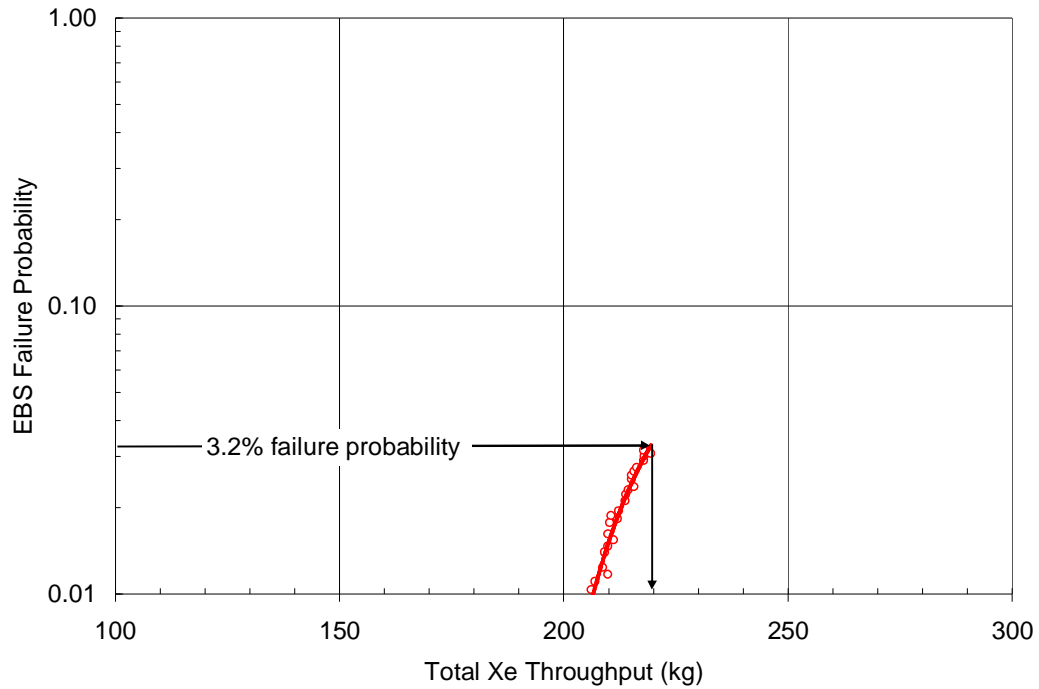


Fig. 37. Calculated failure probability for FT1 to complete the mission for the 1% of cases where FT2 failed after processing 178 kg of xenon. This assume that only FT1 and FT2 are used for the entire mission and that prior to the failure of FT2 the thrusters were shared the propellant throughput equally at every throttle level.